



## Atmospheric Deposition of Reactive Nitrogen to a Deciduous Forest in the Southern Appalachian Mountains

John T. Walker<sup>1</sup>, Xi Chen<sup>1a</sup>, Zhiyong Wu<sup>1b</sup>, Donna Schwede<sup>1</sup>, Ryan Daly<sup>1c</sup>, Aleksandra Djurkovic<sup>1</sup>, A. Christopher Oishi<sup>2</sup>, Eric Edgerton<sup>3</sup>, Jesse Bash<sup>1</sup>, Jennifer Knoepp<sup>2§</sup>, Melissa Puchalski<sup>4</sup>, John Iames<sup>1</sup>, Chelcy F. Miniati<sup>2d</sup>

<sup>1</sup>U.S. Environmental Protection Agency, Office of Research and Development, Durham, NC, USA

<sup>2</sup>U.S. Department of Agriculture, Forest Service, Otto, NC, USA

<sup>3</sup>Atmospheric Research and Analysis, Inc., Cary, NC, USA

10 <sup>4</sup>U.S. Environmental Protection Agency, Office of Air and Radiation, Washington, DC, USA

<sup>a</sup>Now at: U.S. Environmental Protection Agency, Office of Air Quality Planning and Standards, Durham, NC, USA

<sup>b</sup>Now at: RTI International, Durham, NC, USA

<sup>c</sup>Now at: Boulder A.I.R. LLC, Boulder, CO, USA

<sup>d</sup>Now at: U.S. Department of Agriculture, Forest Service, Albuquerque, NM, USA

15 <sup>§</sup>Recently retired

Correspondence to: John T. Walker (walker.johnt@epa.gov)

**Abstract.** Assessing nutrient critical load exceedances requires complete and accurate atmospheric deposition budgets for reactive nitrogen ( $N_r$ ). The exceedance is the total amount of  $N_r$  deposited to the ecosystem in excess of the critical load, which is the amount of  $N_r$  input below which harmful effects do not occur. Total deposition includes all forms of  $N_r$  (i.e., organic and inorganic) deposited to the ecosystem by wet and dry pathways. Here we present results from the Southern Appalachian Nitrogen Deposition Study (SANDS), in which a combination of measurements and field-scale modeling were used to develop a complete annual  $N_r$  deposition budget for a deciduous forest at the Coweeta Hydrologic Laboratory. Wet deposition of ammonium, nitrate, nitrite, and bulk organic N were measured directly. The dry deposited  $N_r$  fraction was estimated using a bidirectional resistance-based model driven with speciated measurements of  $N_r$  air concentrations (e.g., ammonia, ammonium aerosol, nitric acid, nitrate aerosol, bulk organic N in aerosol, total alkyl nitrates, and total peroxy nitrates), micrometeorology, canopy structure, and biogeochemistry. Total annual deposition was  $\sim 6.6 \text{ kg N ha}^{-1} \text{ yr}^{-1}$ , which is on the upper end of  $N_r$  critical load estimates recently developed for similar ecosystems in nearby Great Smoky Mountains National Park. Of the total (wet + dry) budget, 50.7% was contributed by reduced forms of  $N_r$  ( $\text{NH}_x = \text{ammonia} + \text{ammonium}$ ), with oxidized and organic forms contributing  $\sim 41.6\%$  and  $7.7\%$ , respectively. Our results indicate that reductions in  $\text{NH}_x$  deposition would be needed to achieve the lowest estimates ( $\sim 3.0 \text{ kg N ha}^{-1} \text{ yr}^{-1}$ ) of  $N_r$  critical loads in southern Appalachian forests.



## 1 Introduction

35 Prior to the Industrial Revolution, Earth's ecosystems received reactive nitrogen ( $N_r$ ) deposition rates of  $\sim 0.5 \text{ kg ha}^{-1} \text{ yr}^{-1}$  (Holland et al., 1999). Since the 19<sup>th</sup> century, anthropogenic activities, both industrial and agricultural, have resulted in unprecedented quantities of  $N_r$  being released into the atmosphere, subsequently altering biogeochemical cycles (Neff et al., 2002a,b; Ollinger et al., 2002; Bragazza et al., 2006; Doney et al., 2007; Galloway et al., 2008; Boonstra et al., 2017). Excessive atmospheric deposition of  $N_r$  to terrestrial ecosystems may lead to soil and aquatic acidification, nutrient imbalance and enrichment, plant damage and microbial community changes as well as loss of biodiversity (Bobbink et al., 1998; Lohse et al., 2008; Simkin et al., 2016). Nitrogen deposition rates in many areas now exceed  $10 \text{ kg ha}^{-1} \text{ yr}^{-1}$  and may double current rates by the year 2050 in some regions (Galloway et al., 2008). The amount of  $N_r$  deposition below which significant harmful effects do not occur is known as the critical load (Nilsson and Grennfelt, 1988). Critical loads can be quantified using empirical relationships between ecosystem  $N$  input and ecosystem response (Pardo et al., 2011; Root et al., 2015), or mass balance type biogeochemical models (Lynch et al., 2017; McNulty et al., 2007). For the southern Appalachian Mountains, simple mass balance approaches yield critical loads similar to those derived from empirical approaches for forest health and biogeochemical responses. In a recent study employing a mass balance model for the Great Smoky Mountains National Park, Pardo et al. (2018) quantified critical loads for spruce-fir, beech, and mixed deciduous forests in the range of  $2.8$  to  $7 \text{ kg N ha}^{-1} \text{ yr}^{-1}$ , with the highest value corresponding to a high-elevation spruce-fir site experiencing disturbance-induced regrowth. Accurate and complete deposition budgets (i.e., including all forms of  $N$ ) are required to quantify the amount of  $N$  input to ecosystems in excess of the critical load (i.e., the critical load exceedance). Estimates of  $N$  deposition for critical load assessments can be derived from gridded chemical transport models (CTMs) (Ellis et al., 2013; Lee et al., 2016; Simkin et al., 2016; Clark et al., 2018; Makar et al., 2018), measurement-model fusion (MMF) techniques that combine measurements with CTM output (Schwede and Lear, 2014; Nanus et al., 2017; McDonnell et al., 2018; U.S. EPA, 2019a), or inferential modeling with site specific measurements (Flechard et al., 2011; Li et al., 2016). While these approaches reflect the state-of-the-science and are widely used, they collectively suffer from incompleteness of the  $N$  deposition budget (and are therefore biased low) (Walker et al., 2019a). Monitoring networks for wet deposition (NADP/NTN) and air concentrations of  $N_r$  (CASTNET) focus only on inorganic species, excluding organic forms of  $N$  which account for  $\sim 25\%$  of total  $N$  in wet deposition on average (Jickels et al., 2013). Due to difficulties in sampling (Walker et al., 2012) and the inability to fully speciate the wide range of constituents (Neff et al., 2002a; Altieri et al., 2009, 2012; Cape et al., 2011; Samy et al., 2013; Chen et al., 2018), organic  $N$  is not routinely monitored. Hence, deposition of organic  $N$  remains uncertain, and thus  $N$  deposition budgets developed from network monitoring data and CTMs remain incomplete. Current  $N$  deposition estimates also have a relatively high degree of uncertainty in the estimation of dry deposition. While wet deposition is routinely measured, direct measurements of dry  $N_r$  deposition (i.e., flux measurements) in North America are relatively few (Walker et al., 2020). Estimates of dry deposition for ecosystem assessments is therefore derived from models (Schwede and Lear, 2014; Li et al., 2016; Lee et al., 2016). Of the inorganic  $N$  species,  $\text{NH}_3$  is the most important contributor to dry deposition in many areas (Walker et al., 2019b) but also the most



70 uncertain (Flechard et al., 2011) due to the bi-directionality of surface-atmosphere exchange. A paucity of flux measurements (Walker et al., 2020) precludes bias correction of dry deposition in CTMs and MMF techniques, making dry deposition much more uncertain relative to wet deposition.

The Coweeta study site represents southern Appalachian Mountain forests, highly diverse and productive ecosystems that provide a variety of ecosystem services, including a source of surface drinking water (Caldwell et al., 2014).  
75 While deposition of oxidized N to forests in the southeastern U.S. has declined in response to the Clean Air Act, montane ecosystems continue to receive high rates of deposition due to elevation-induced precipitation gradients (Weathers et al., 2006; Knoepp et al., 2008). Southern Appalachian forests continue to show signs of sensitivity to N deposition. For example, litterfall N fluxes and foliar N concentrations at Coweeta have steadily increased over the past two decades (Knoepp et al., 2018). Highly spatially variable meteorological patterns typical of complex terrain  
80 are difficult to model (Lehner and Rotach, 2018), leading to uncertainties in precipitation amounts and wet deposition (Zhang et al., 2018) as well as the micrometeorological processes that govern dry deposition. Estimates of deposition from gridded CTMs in mountainous terrain therefore contain a higher degree of uncertainty relative to low-elevation ecosystems. For these reasons, a better understanding of total N deposition in southern Appalachian forests is needed. This study investigates the N deposition budget in a remote montane forest in the southeastern U.S. We combine  
85 measurements of wet deposition, speciated air concentrations of  $N_r$ , micrometeorology, biogeochemistry and forest canopy structure with in-situ inferential dry deposition modeling to develop an annual, speciated, total N deposition budget, including net and component  $NH_3$  fluxes as well as dry and wet organic N deposition. Seasonal and annual total N deposition fluxes are presented in the context of long-term trends in air concentrations and wet deposition of inorganic N species. Spatial representativeness is characterized using measurements of air concentrations of the  
90 primary inorganic N species and previous wet deposition measurements along an elevation gradient across the topographically complex forested basin.

## 2 Methods

### 2.1 Site description

The study was conducted at the USDA Forest Service Coweeta Hydrologic Laboratory, a 2,185-ha experimental forest in southwestern North Carolina, USA (35°3' N, 83°25' W) near the southern end of the Appalachian Mountain  
95 chain. Topography is complex, with elevations ranging from 675 to 1592 m within the Coweeta Basin. Mean annual temperature and precipitation are 12.9 °C and 1795 mm, respectively. Dominant overstory species are *Liriodendron tulipifera*, *Quercus alba*, *Betula lenta*, and *Acer rubrum*, which comprise 24%, 17%, 11%, and 8% of the basal area, respectively, in the low-elevation forests where the study was conducted (Oishi et al., 2018). The dominant understory woody shrub species is *Rhododendron maximum* (evergreen), which comprises 13% of the basal area (Oishi et al.,  
100 2018). Species composition in the vicinity of the eddy flux tower (EFT), further described below, is detailed in Table S1. Canopy height surrounding the EFT is ~ 30 m.

The Coweeta Basin has been a long-term monitoring site for atmospheric chemistry and deposition since the late 1970s. Weekly wet deposition of ammonium ( $NH_4^+$ ) and nitrate ( $NO_3^-$ ), along with sulfate ( $SO_4^{2-}$ ), chloride, and base



105 cations have been measured as part of the NADP/NTN (Site NC25, <https://nadp.slh.wisc.edu/networks/national-trends-network/>) since 1978. Weekly integrated air concentrations of particulate  $\text{NH}_4^+$ ,  $\text{NO}_3^-$ ,  $\text{SO}_4^{2-}$ , chloride, and base cations, as well as nitric acid ( $\text{HNO}_3$ ) and sulfur dioxide ( $\text{SO}_2$ ), have been measured by CASTNET (Site COW137, <https://www.epa.gov/castnet>) since 1987. Since 2011, bi-weekly integrated air concentrations of ammonia ( $\text{NH}_3$ ) have been measured by the NADP Ammonia Monitoring Network (AMoN Site NC25, <https://nadp.slh.wisc.edu/networks/ammonia-monitoring-network/>). Here we use these datasets to place our study  
110 results into historical context, supplement the more intensive atmospheric chemistry measurements described below, and as inputs for inferential modeling of dry deposition. The long-term NADP and CASTNET measurements are collected in the lower part of the basin, indicated as NC25/COW137 in Figure 1.

## 2.2 Southern Appalachian Nitrogen Deposition Study

115 Building on the long-term NADP and CASTNET measurements described above, the Southern Appalachian Nitrogen Deposition Study (SANDS) was conducted in 2015 and 2016 to better understand the atmospheric chemistry and deposition of reactive nitrogen at Coweeta. Intensive measurement campaigns were conducted from May 21–June 9, 2015; August 6–25, 2015; September 9–26, 2015; April 19–May 11, 2016; and July 13–August 3, 2016. A subset of measurements was conducted continuously between May 2015 to August 2016. As described below, time-resolved and time-integrated measurement techniques were used to characterize organic N in the gas phase, in particulate  
120 matter, and in wet deposition; the temporal variability of air concentrations of gas-phase oxidized and reduced forms of N; and the spatial variability of atmospheric N concentrations across the Coweeta Basin. Vertical profiles of air concentrations were measured within the forest canopy to examine source/sink processes and measurements of soil and vegetation chemistry were conducted to characterize  $\text{NH}_3$  emission potentials. Measurements were combined with NADP and CASTNET data to develop seasonal and annual total N deposition budgets employing inferential modeling  
125 for the dry deposition component. Vertical concentration profile and biogeochemical measurements were used to inform the parameterization of  $\text{NH}_3$  bi-directional exchange. Sampling locations are described in Figure 1 and Table 1. Measurement details are summarized in Table 2.

### 2.2.1 Wet deposition

130 Additional wet deposition measurements were conducted adjacent to the NTN NC25 sampler to quantify the contribution of bulk water-soluble organic N (WSON) to water-soluble total nitrogen (WSTN) in precipitation. Weekly precipitation samples were collected in a modified wet-only sampler with a borosilicate glass funnel and amber glass bottle (Walker et al., 2012), shielded from sunlight, and maintained in the field under continuous refrigeration to maintain the stability of ON until retrieval (Walker et al., 2012). Samples were sent to the NADP Central Analytical Laboratory on ice for analysis of  $\text{NH}_4^+$ ,  $\text{NO}_3^-$ ,  $\text{NO}_2^-$ , and WSTN as described by Walker et al.  
135 (2012). WSON concentration was calculated as:  
$$\text{WSON} = \text{WSTN} - (\text{NH}_4^+ + \text{NO}_3^- + \text{NO}_2^-) \quad (1)$$

The method detection limit for WSON is  $10 \mu\text{g N L}^{-1}$  (Walker et al., 2012). These measurements were collected continuously from February 2015 to August 2016.



140 During the spring of 2015, thymol was added to the precipitation collection bottle as a biocide to inhibit organic  
nitrogen loss in the sample should the refrigerated collector malfunction or lose power. Thymol negatively affected  
the precision of the total nitrogen measurement, and its use was discontinued in fall of 2015. Ultimately, there were  
no issues with the refrigerated collector, and the thymol-containing samples were excluded from the analysis presented  
herein. However, this data loss resulted in a gap from August 2015 to mid-October 2015 of the 12-month period for  
which the total deposition budget is developed. The data gap comprised eight weekly periods in which precipitation  
145 occurred. For this period, the  $\text{NH}_4^+$  and  $\text{NO}_3^-$  concentrations from the collocated NADP/NTN NC25 sampler were  
used. Based on the SANDS measurements, the ON concentration during this period was estimated by assuming that  
 $\text{NH}_4^+ + \text{NO}_3^-$  contribute 89% of total nitrogen in rainfall, with WSON representing the balance (11%). For the annual  
budget, weekly concentrations were combined with measured precipitation depth to calculate weekly deposition ( $\text{kg}$   
 $\text{N ha}^{-1}$ ). Comparison between SANDS and NTN concentrations of  $\text{NH}_4^+$  and  $\text{NO}_3^-$  showed very good agreement  
150 (Supplemental Section S1, Figure S1).

### 2.2.2 Air concentrations

Hourly concentrations of  $\text{NO}_y$ ,  $\text{HNO}_3$ , total gas-phase peroxy nitrates ( $\Sigma\text{PN}$ ), and total gas-phase alkyl nitrates ( $\Sigma\text{AN}$ )  
were measured continuously from August 2015 to August 2016 at the height of 8 m adjacent to the COW137  
CASTNET tower (Figure 1, Tables 1 and 2).  $\text{NO}_y$  and  $\text{HNO}_3$  were measured using a modified model 42S  $\text{NO}-\text{NO}_2-$   
155  $\text{NO}_x$  analyzer; the  $\text{NO}_y$  technique is described in detail by Williams et al. (1998). Briefly, total oxidized reactive  
nitrogen ( $\text{NO}_y$ ) is converted to  $\text{NO}$  using a molybdenum catalyst heated to 325 °C. On a second channel, a metal  
denuder coated with potassium chloride ( $\text{KCl}$ ) is used to remove  $\text{HNO}_3$  before passing through a second molybdenum  
converter heated to 325 °C. The difference between the total  $\text{NO}_y$  measurement and the  $\text{HNO}_3$ -scrubbed  $\text{NO}_y$   
measurement is interpreted as  $\text{HNO}_3$ . Here we refer to the method as denuder difference chemiluminescence (DD-  
160 CL).

Total peroxy nitrates ( $\Sigma\text{PNs}$ ) and total alkyl nitrates ( $\Sigma\text{ANs}$ ) were measured using a modification of the technique  
described by Day et al. (2002), in which  $\text{PNs}$  and  $\text{ANs}$  are thermally decomposed to  $\text{NO}_2$  (plus an organic radical),  
followed by measurement of the incremental  $\text{NO}_2$  above ambient background for each decomposition step. Day et al.  
(2002) quantified  $\text{NO}_2$  via laser induced fluorescence, while photolytic conversion to  $\text{NO}$  and quantification of the  
165 resulting  $\text{NO}$  by  $\text{NO}-\text{O}_3$  chemiluminescence is used in the current study. Here we refer to the method as thermal  
decomposition, photolytic conversion, chemiluminescence (TD-PC-CL). A single chemiluminescence analyzer was  
used for  $\text{NO}_y$ ,  $\text{HNO}_3$ ,  $\Sigma\text{PN}$ , and  $\Sigma\text{AN}$  measurements. Additional detail on the instrument and associated QA/QC  
procedures is included in Supplemental Section S2.

Hourly concentrations of  $\text{NH}_3$  and  $\text{HNO}_3$  were measured on the eddy flux tower (EFT, Figure 1, Tables 1 and 2) at  
170 two heights above the canopy (34 m and 37.5 m above ground during spring, 2016; 34 m and 43.5 m above ground  
during summer, 2016) using the Monitor for Aerosols and Gases in Ambient Air (MARGA, Metrohm Applikon B.V.,  
the Netherlands). Details and principles of the MARGA system have been previously described (Rumsey and Walker,  
2016; Chen et al., 2017). Briefly, the MARGA 2S consisted of two sampler boxes positioned on the tower and a  
detector box located in a climate-controlled enclosure at the base of the tower. Sample boxes comprised an inlet of



175 1.27 cm outer diameter 30 cm long PFA Teflon tubing with no particle size selection, through which air flow was  
mass controlled at  $\sim 16.7 \text{ L min}^{-1}$ , a wet rotating denuder (WRD) for collection of soluble gases, and a steam jet aerosol  
collector (SJAC). Liquid sample from the WRD and SJAC is continuously drawn from the sample boxes down the  
tower to the analytical box for analysis Ion Chromatography (IC) on an hourly basis at the detector unit located in a  
climate-controlled enclosure at the base of the tower. At the beginning and end of the measurement intensive, multi-  
180 level liquid  $\text{NO}_3^-$  and  $\text{NH}_4^+$  standards were introduced at the WRD and SJAC, with airflow turned off, to assess the  
analytical accuracy of the  $\text{NH}_3$  and  $\text{HNO}_3$  measurement. MARGA measurements were conducted during the spring  
and summer of 2016 intensives. Comparisons of continuous and time-integrated methods for  $\text{HNO}_3$  and  $\text{NH}_3$  are  
summarized in Supplemental Section S1 (Figures S2 and S3).

Concentrations of  $\text{NH}_3$ ,  $\text{HNO}_3$ ,  $\text{SO}_2$ ,  $\text{NH}_4^+$ ,  $\text{NO}_3^-$ , and  $\text{SO}_4^{2-}$  in air were measured concurrently on the EFT at 10 heights  
185 from just above the forest floor (0.5 m above ground) to several meters above the canopy (upper height of 37 m above  
ground during spring 2016, 43.5 m above ground during summer, 2016) using a glass annular denuder/filter pack  
(URG Corporation, Chapel Hill, NC) system. The sampling assembly included a 1%  $\text{Na}_2\text{CO}_3$  coated denuder for  
collection of acid gases followed by a 1%  $\text{H}_3\text{PO}_3$  coated denuder for collection of  $\text{NH}_3$ , and a filter pack containing a  
primary Teflon filter for collection of aerosol and a backup Nylon filter (47 mm, Pall Corp, Port Washington, NY) to  
190 collect  $\text{HNO}_3$  liberated by dissociation of  $\text{NH}_4\text{NO}_3$  on the primary filter. Inlets were Teflon coated glass impactors  
with a nominal  $2.5 \mu\text{m}$  aerodynamic diameter cutpoint (URG Corporation, Chapel Hill, NC). Sample durations were  
typically 3 or 4 h at a flow rate of  $\sim 16.7 \text{ L min}^{-1}$ . Flow rates were controlled by critical orifice and were verified  
before and after each sampling period with a NIST traceable primary standard flow meter (Bios DryCal DC-Lite  
flowmeter, Mesa Laboratories, Inc., Lakewood, CO).

195 Denuders and filters were extracted with 10 mL of deionized water and analyzed by ion chromatography (IC, Dionex  
model ICS-2100, Thermo Scientific, Waltham, MA). Extracts were analyzed for cations using Dionex IonPac 2-mm  
CG12 guard and CS12 analytical columns; separations were conducted using 20 mM methanesulfonic acid (MSA) as  
eluent at a flow rate of  $0.25 \text{ mL min}^{-1}$ . Anions were analyzed (IonPac 2-mm AG23 guard column, AS23 analytical  
columns) using an isocratic eluent mix of carbonate/bicarbonate (4.5/0.8mM) at a flow rate of  $0.25 \text{ mL min}^{-1}$ . Multi-  
200 point ( $\geq 5$ ) calibrations were conducted using a mixture prepared from individual inorganic standards (Inorganic  
Ventures, Christiansburg, VA). A mid-level accuracy check standard was prepared from certified standards mix  
(AccuStandard, New Haven, CT) for quality assurance/quality control. Profile measurements were conducted during  
each of the five SANDS intensives.

Bulk organic nitrogen in aerosols was measured using a high-volume (Hi-Vol) Tisch TE-1000 (Tisch Environmental,  
205 Cleves, OH) dual cyclone  $\text{PM}_{2.5}$  sampler operated at a flow rate of  $230 \text{ L min}^{-1}$ . The unit was deployed at ground level  
adjacent to the COW137 CASTNET tower and collected 24 h (started at 7 A.M. local time) integrated samples on  
pre-baked ( $550 \text{ }^\circ\text{C}$  for 12 h) quartz fiber (QF) filters (90-mm, Pall Corp, Port Washington, NY). Field blanks were  
collected the same way except being loaded in the sampler without the pump switched on. A QF punch ( $1.5 \text{ cm}^2$ ) from  
each sample was extracted with DI water ( $18.2 \text{ M}\Omega\text{-cm}$ , Milli-Q Reference system, Millipore, Burlington, MA) in an  
210 ultrasonic bath for 45 min. The sample extract was filtered through a  $0.2\text{-}\mu\text{m}$  pore size PTFE membrane syringe filter  
(Iso-disc, Sigma Aldrich, St. Louis, MO) before subsequent analyses.



Water-soluble total N (WSTN) concentrations were measured using a high-temperature catalytic combustion and chemiluminescence method that included a total organic carbon analyzer (TOC-VCSH) combined with a total nitrogen module (TNM-1) (Shimadzu Scientific Instruments, Columbia, MD). Briefly, the TN module converts all nitrogen compounds to NO at 720 °C in a combustion chamber, and NO is quantified by NO<sub>2</sub> chemiluminescence through reaction with ozone. A 5-point calibration was conducted with KNO<sub>3</sub> standard solution for each batch of samples. Before and after each batch of samples being analyzed, a suite of quality assurance check analysis including lab DI and accuracy check standard were conducted to ensure accuracy and precision. Inorganic species (NH<sub>4</sub><sup>+</sup>, NO<sub>3</sub><sup>-</sup>, NO<sub>2</sub><sup>-</sup>) were analyzed by IC as described above, and WSON was calculated according to equation (1). Comparisons of time HiVol and CASTNET PM measurements are summarized in Supplemental Section S1 (Figure S4).

To evaluate the spatial distribution of gaseous N across the Coweeta Basin, additional passive sampling of HNO<sub>3</sub> and NH<sub>3</sub> was conducted across an elevation gradient for the full year of 2015 (Figure 1, Tables 1 and 2). Samplers were deployed for two-week periods at the height of 10 m above ground on an aluminum tilt-down tower. NH<sub>3</sub> measurements followed AMoN methods. HNO<sub>3</sub> was collected on 47-mm Nylon filters (Nylasorb, Pall Corp, Port Washington, NY) as described by Bytnerowicz et al. (2005). NH<sub>3</sub> and HNO<sub>3</sub> sampler preparation and analysis was performed by the NADP Central Analytical Laboratory and CASTNET laboratories, respectively. Field calibration of the passive HNO<sub>3</sub> measurements (Supplemental Figure S5) was based on comparison with a collocated CASTNET sampler at Screwdriver Knob site (Figure 1, Tables 1 and 2), which also operated for the full year of 2015. Air concentrations derived from passive samplers were corrected for temperature and pressure.

### 2.2.3 Micrometeorology

Site characteristics of micrometeorology and ecosystem fluxes of water and carbon dioxide have been previously described (Novick et al., 2013; 2014; Oishi et al., 2018). Three-dimensional wind components were measured by sonic anemometer (Model 81000, R.M. Young Company, Traverse City, MI) above the forest canopy on the EFT. Momentum and kinematic heat fluxes were determined by eddy covariance (EC) from sonic data. For EC calculations, raw 10-Hz sonic data were processed into hourly averages after block average detrending and 2D coordinate rotation (Novick et al., 2013). Air temperature and relative humidity were measured at the top of the tower (EC155, Campbell Scientific, Logan, UT) and 2/3 canopy height (HMP-45, Vaisala, Helsinki, Finland). Photosynthetically active radiation (PAR; LI-190, LI-COR Biosciences, Lincoln, NE) and upward and downward, shortwave and longwave radiation (CNR 4, Kipp & Zonen, Delft, The Netherlands) were measured at the top of the tower. Surface wetness was measured in the canopy crown, understory and at the ground using leaf wetness sensors (Model 237, Campbell Scientific). Soil volumetric water content (VWC) averaged over 0–30 cm depth was measured in four locations around the tower using time domain reflectometry probes (CS616, Campbell Scientific). Soil temperature was measured at four depths (5, 20, 35, and 55 cm) in two locations near the tower using thermistors. For missing data, linear interpolation was used to fill short gaps (1–4 h). Longer gaps were filled by substitution using the average hourly diel profile calculated for each month. Micrometeorological data were used for inferential dry deposition modeling as described below.



## 2.2.4 Biogeochemistry

Ammonia emission potentials ( $\Gamma$ ) and compensation points for live vegetation, leaf litter on the forest floor, and soil were estimated from measurements of  $\text{NH}_4^+$  and pH in the leaf and litter tissue and soil pore water (Massad et al., 2010). Green leaves were collected from 18 species (Table S1) within the flux footprint of the tower and other locations in the Coweeta Basin. Leaf litter was collected along transects extending to the northeast and southwest (i.e., predominant wind directions) of the flux tower ~100 m. Litter included a composite of intact leaves and leaf fragments and excluded the more decomposed material at the top of the organic soil layer. Approximately 5 g of leaf tissue was ground in liquid nitrogen using a mortar and pestle and small coffee grinder, then extracted with 20 mL of deionized water. pH was determined directly on the extracts (Oakton pH 2100 meter, Mettler Toledo InLab Micro electrode). The  $[\text{NH}_4^+]$  in the extracts, which reflects the bulk tissue concentration, was determined by ion chromatography as described above for denuder measurements either directly or, for samples with high organic content, after separation of the  $\text{NH}_4^+$  from the solution as  $\text{NH}_3$  using headspace equilibration. For the headspace method, 5 mL of tissue extract was added to a 250-mL high-density polyethylene jar containing two ALPHA passive samplers (Center for Ecology and Hydrology; Tang et al., 2001), without the diffusion barrier, affixed to the interior of the lid. The jar was sealed, and 5 mL of 0.3 N NaOH was added to the extract via a septum. The  $\text{NH}_3$  liberated from the liquid extract into the headspace was collected by the passive diffusion samplers over a period of 48 h, after which the passive sampler was extracted with 10 mL of deionized water. Extracts were then analyzed by ion chromatography as described above. Emission potentials of the vegetation ( $\Gamma_s$ ) and litter ( $\Gamma_l$ ) were estimated from measured concentrations of  $[\text{H}^+]$  (M) and  $[\text{NH}_4^+]$  ( $\mu\text{g g}^{-1}$  tissue fresh weight) in the bulk tissue as:

$$\Gamma_{s,l} = \frac{[\text{NH}_4^+] \times (5.56E^{-5}) \times LD}{[\text{H}^+]} \quad (2)$$

where LD is leaf density ( $\text{kg L}^{-1}$  fresh tissue, equivalent to  $\text{g cm}^{-3}$  fresh tissue). In this case, LD for woody deciduous and woody evergreen species are 0.37 and 0.42  $\text{kg L}^{-1}$ , respectively (Poorter et al., 2009). Emission potentials for litter, which consisted of a mix of in-tact or partial leaves and needles, assume an average density of 0.4  $\text{kg L}^{-1}$ . The factor of 5.56E-5 in equation 2 is necessary to convert  $[\text{NH}_4^+]$  from  $\mu\text{g NH}_4^+ \text{g}^{-1}$  tissue to  $\text{mol NH}_4^+ \text{kg tissue}^{-1}$ .

Soil chemistry was measured in 20 m x 20 m plots located in the vicinity of the tower. During 2010, soil  $\text{NH}_4^+$  was determined on soil samples collected with PVC cores (5-cm diameter and 10-cm deep) in four locations (replicates) within each of four plots. Samples were collected bi-monthly during the growing season.  $\text{NH}_4^+$  was extracted within two hours of collection using 5 g of sieved (<5 mm) soil in 20 mL of 2M potassium chloride followed by colorimetric analysis (Astoria2 autoanalyzer, Astoria-Pacific International; Coweeta Hydrologic Laboratory, 2016). Soil pH was measured on 0–10 cm samples collected in three plots in winter of 2013 (each sample representing a composite of 20–25 2.5-cm diameter soil cores). Soil pH was determined directly after mixing 5 g soil with 10 mL 0.01M calcium chloride (Coweeta Hydrologic Laboratory, 2016). Soil emission potential ( $\Gamma_{\text{soil}}$ ) (unitless) was estimated directly from measured molar concentrations of  $[\text{H}^+]$  and  $[\text{NH}_4^+]$  as:

$$\Gamma_g = \frac{[\text{NH}_4^+]}{[\text{H}^+]} \quad (3)$$





### 2.2.5 Above-canopy flux measurements

Above-canopy fluxes of  $\text{NH}_3$  and  $\text{HNO}_3$  were quantified from measurements of vertical concentration gradients conducted during the final (summer 2016) intensive when the tower was at maximum height and the greatest vertical separation of concentration measurements was achieved. Fluxes were determined using the modified Bowen-ratio (MBR) method (Meyers et al., 1996) as:

$$F = -K_c(z) \frac{dC}{dz}, \quad (4)$$

where  $K_c$  and  $dC/dz$  are the eddy diffusivity and vertical concentration gradient of the chemical species of interest. The value of  $K_c$  for trace gases was assumed equivalent to the eddy diffusivity of heat ( $K_t$ ), calculated as:

$$K_c = K_t = -\overline{w't'} \frac{\Delta z}{\Delta t}, \quad (5)$$

where  $\overline{w't'}$  is the kinematic surface heat flux measured above the canopy (43.5 m above ground level),  $\Delta t$  is the air temperature difference between the levels at 43 m and 35 m above ground level, and  $\Delta z$  is the height interval of air temperature measurements. Air temperature was measured using aspirated thermocouples, and  $\Delta t$  was corrected for a small bias between the sensors determined by collocated comparison. Concentration gradients were determined from URG annular denuder measurements at 34.6 m and 43 m above ground level, as described above in section 2.2.2. Given the complexity of the topography, no attempt was made to correct for potential roughness sub-layer effects on either the eddy diffusivity or concentration gradients, which should be acknowledged as a source of uncertainty in the calculated  $\text{HNO}_3$  and  $\text{NH}_3$  fluxes. Additional detail on the gradient measurements is included in Supplemental Section S3.

### 2.2.6 Seasonal and annual deposition budget

Speciated seasonal and annual total nitrogen deposition budgets were developed for the period August 2015 to August 2016. The wet deposited components, including  $\text{NH}_4^+$ ,  $\text{NO}_3^-$ , and total WSON, were directly measured. Speciated dry deposition was estimated by combining measured air concentrations, micrometeorology, biogeochemistry and canopy physical characteristics within a box version of the Surface Tiled Aerosol and Gaseous Exchange (STAGE) model, which is an option in the Community Multi-scale Air Quality Model (CMAQ) version 5.3 (Appel et al., 2021). The STAGE model treats the deposition of gases and particles separately. The air-surface exchange of gases is parameterized as a gradient process and is used for both bidirectional exchange and dry deposition following the widely used resistance model of Nemitz et al. (2001) and Massad et al. (2010):

$$F = -f_{veg} \frac{\chi_a(z) - \chi_{z0}}{R_a} - (1 - f_{veg}) \frac{\chi_a(z) - \chi_g}{R_a + R_g}, \quad (6)$$

where  $F$  is the net flux above the canopy (a negative value represents a net deposition flux and a positive value represents a net emission flux),  $\chi_a(z)$  is the ambient concentration at a reference height ( $z$ ),  $\chi_{z0}$  is the concentration at height  $d$  (displacement height) +  $z_0$  (roughness length),  $\chi_g$  is the ground layer compensation point,  $R_a$  is the aerodynamic resistance between  $z$  and  $d + z_0$  is  $R_a$ ,  $R_g$  is the total ground resistance including in-canopy aerodynamic resistance ( $R_{inc}$ ), ground boundary layer resistance ( $R_{bg}$ ), and soil resistance ( $R_{soil}$ ) ( $R_g = R_{inc} + R_{bg} + R_{soil}$ ), and  $f_{veg}$  is



the vegetation coverage fraction. The ground is fully covered by vegetation at our forested site, and  $f_{veg}$  is therefore set to 1.

The quantity  $\chi_{z0}$  is related to the canopy ( $\chi_c$ ) and ground compensation points ( $\chi_g$ ) according to:

$$\chi_{z0} = \frac{\left(\frac{\chi_a(z)}{R_a} + \frac{\chi_c}{R_{bl}} + \frac{\chi_g}{R_g}\right)}{\left(\frac{1}{R_a} + \frac{1}{R_{bl}} + \frac{1}{R_g}\right)}, \quad (7)$$

where  $R_{bl}$  is the leaf boundary layer resistance.  $\chi_c$  follows Nemitz et al. (2001) but is modified to account for a cuticular compensation point ( $\chi_{cut}$ ):

$$\chi_c = \frac{\chi_a(z)(R_a R_{bl})^{-1} + \chi_s \left[ (R_a R_s)^{-1} + (R_{bl} R_s)^{-1} + (R_g R_s)^{-1} \right] + \chi_{cut} \left[ (R_a R_{cut})^{-1} + (R_{bl} R_{cut})^{-1} + (R_g R_{cut})^{-1} \right] + \chi_g (R_{bl} R_g)^{-1}}{(R_a R_{bl})^{-1} + (R_a R_s)^{-1} + (R_a R_{cut})^{-1} + (R_{bl} R_s)^{-1} + (R_{bl} R_{cut})^{-1} + (R_g R_s)^{-1} + (R_g R_{cut})^{-1}}, \quad (8)$$

where  $\chi_s$  is the leaf stomatal compensation point, and  $R_s$  and  $R_{cut}$  are the stomatal and cuticular resistances, respectively.

The stomatal, cuticular, and ground compensation points ( $\chi_s$ ,  $\chi_{cut}$ ,  $\chi_g$ ) are described according to Nemitz et al. (2000a) as a function of temperature ( $T$ ) and the emission potentials ( $\Gamma$ ):

$$\chi_{s,cut,g} = \frac{161512}{T} 10^{\frac{-4507.11}{T}} \Gamma_{s,cut,g}. \quad (9)$$

$\Gamma_{cut}$  is set to 0 in this study, and thus, there is only deposition to leaf cuticles. For unidirectional exchange of gases other than  $\text{NH}_3$ ,  $\Gamma_s$  and  $\Gamma_g$  are also set to 0. In the case of  $\text{NH}_3$ , the foliage and ground layers may act as a source or sink depending on the ratio of the ambient concentration to the respective compartment compensation point (Husted and Schjoerring, 1995). Here values of  $\Gamma$  for  $\text{NH}_3$  are derived from measurements of live vegetation, litter, and soil chemistry as described above. Values used in the base model simulation are described in Section 3.6, and the sensitivity of modeled  $\text{NH}_3$  fluxes to  $\Gamma$  is discussed in Supplemental Section S5.

Formulas for each resistance component are summarized in Supplemental Table S2. The resistances are largely estimated following Massad et al. (2010) with the following exceptions. The value of  $R_s$  is based on the Noah (Chen and Dudhia, 2001) or P-X land surface schemes (Pleim and Xiu, 1995) in the Weather Research and Forecasting (WRF) model, and in this study, the P-X scheme is used. Deposition to wetted cuticular and ground surfaces considers the bulk accommodation coefficient, following Fahey et al. (2017), and can be a limiting factor for highly soluble compounds. The value of  $R_{mc}$  follows Shuttleworth and Wallace (1985) as does Massad et al. (2010), but uses the canopy momentum attenuation parameterization from Yi (2008) and in-canopy eddy diffusivity following Harman and Finnigan (2007). This parameterization is similar to Bash et al. (2010), and detailed descriptions of model resistance can be found in the references mentioned above.

Dry deposition ( $F$ ) of aerosol nitrogen ( $\text{NH}_4^+$  and  $\text{NO}_3^-$ ) is estimated as the product of the measured concentration ( $C$ ) and the STAGE modeled dry deposition velocity ( $V_d$ ):

$$F = -V_d(z) \times C(z). \quad (10)$$

Aerosol dry deposition processes include gravitational settling, Brownian diffusion, surface impaction, and rebound. Similar to gases, STAGE calculates the averaged  $V_d$  for particles by summing the  $V_d$  over vegetative or non-vegetative



surfaces, weighted by vegetation cover fraction which is = 1 (full coverage) at Coweeta.  $V_d$  for a particle with aerodynamic diameter  $D_p$  is calculated as:

$$350 \quad V_d(D_p) = \frac{V_g}{1 - \exp[-V_g(R_a + R_{bp})]} \quad , \quad (11)$$

where  $R_{bp}$  is the boundary layer resistance for particles, and the gravitational settling velocity ( $V_g$ ) is calculated as:

$$V_g = \frac{\rho D_p^2 g}{18\mu} C_c \quad , \quad (12)$$

where  $\rho$  is the density of the aerosol,  $g$  is the acceleration of gravity,  $\mu$  is the air dynamic viscosity, and  $C_c$  is the Cunningham slip correction factor. The turbulent transport processes are considered similar for gas and aerosol, and  $R_a$  can be formulated based on the similarity theory relationships. Unlike deposition of gases, the boundary layer resistance usually dominates the aerosol deposition process as Brownian diffusion is much slower for particles than molecular diffusion is for gases (Pleim and Ran, 2011). Thus,  $R_{bp}$  depends on the collection efficiency of the surface and can be determined as:

$$365 \quad R_{bp} = \left[ F_f u_* \left( S_c^{-\frac{2}{3}} + E_{im} \right) \right]^{-1} \quad , \quad (13)$$

where  $u_*$  is the friction velocity, and  $S_c$  is the Schmidt number for particles. The quantity  $E_{im}$  represents the collection efficiency by impaction and follows Slinn (1982) for vegetative canopies and Giorgi (1986) for smooth (non-vegetative) surfaces. The quantity  $F_f$  is an empirical correction factor to account for increased deposition in convective conditions, parameterized as:

$$365 \quad F_f = V_{fac} \left( 1 + 0.24 \frac{w_*^2}{u_*^2} \right) \quad , \quad (14)$$

where  $V_{fac}$  is an empirical constant representing the enhanced effects over vegetation canopies. For vegetative canopies,  $V_{fac}$  is equal to the one-sided leaf area index (LAI) with a minimum value of one, and for non-vegetative surface, a value of one is used. The quantity  $w_*$  is the convective velocity scale (Deardorff velocity), defined as:

$$370 \quad w_* = \left( \frac{g}{T_v} z_i \overline{w't'} \right)^{\frac{1}{3}} \quad , \quad (15)$$

where  $T_v$  is virtual air temperature,  $z_i$  is average depth of the mixed layer, and  $\overline{w't'}$  is the measured kinematic surface heat flux.

A bulk  $V_d$  for  $PM_{2.5}$  is obtained by integrating size-resolved  $V_d$  according to the particle size distribution. The size distribution profiles for  $NH_4^+$  and  $NO_3^-$  are from measurements at eight Canadian rural forest sites (Zhang et al., 2008) and the size distribution for particulate organic nitrogen is estimated as an average of that for  $NH_4^+$  and  $NO_3^-$ . Model sensitivities of particle nitrogen fluxes to assumed size distributions are discussed in Supplemental Section S5.

375 The STAGE model is extracted from the CMAQ v5.3 and executed in a one-dimensional mode. The prescribed surface parameters (e.g.,  $z_0$ ,  $d$ ) were modified according to the site conditions. The continuous LAI data were extracted from the MODerate resolution Imaging Spectroradiometer (MODIS) global LAI product (MCD15A2H), which is generated daily at a 500-m spatial resolution, and each data point covers an 8-d period. The MODIS LAI (Supplemental Figure S6) was adjusted using in-situ canopy measurements as described in Supplemental Section S4. Hourly meteorological



380 measurements, including air temperature, relative humidity,  $u^*$ , atmospheric pressure, precipitation rate, global radiation, and soil temperature/moisture, were used to drive STAGE. The Obukhov length, which is defined as:

$$L = -\frac{u_*^3 T_v}{(kgw't)}, \quad (16)$$

where  $k$  is the von Karman constant, was also calculated from micrometeorological measurements.

### 2.2.7 Air concentrations for dry deposition modeling

385 Air concentration data used for dry deposition modeling are summarized in Table 3. Hourly measurements of  $\text{HNO}_3$  by DD\_CL and  $\Sigma\text{AN}$  and  $\Sigma\text{PN}$  by TD-PC-CL were conducted for a full year and were therefore used directly for modeling. Over the 12-month sampling period, 18%, 22%, and 22% of hourly  $\text{HNO}_3$ ,  $\Sigma\text{AN}$ , and  $\Sigma\text{PN}$  concentrations were missing or invalid, respectively. Missing data were replaced with the corresponding hour from the median diel profile comprised of days with > 75% completeness. In order to convert measured  $\Sigma\text{AN}$  and  $\Sigma\text{PN}$  concentrations from  
390 ppb to  $\mu\text{g N m}^{-3}$ , surrogate formulas of nitrooxy-butanol ( $\text{C}_4\text{H}_{10}\text{NO}_4$ ) and PAN ( $\text{C}_2\text{H}_3\text{NO}_5$ ) were assumed for  $\Sigma\text{AN}$  and  $\Sigma\text{PN}$ , respectively. The CMAQ V5.2.1 output for Coweeta showed that these were the most abundant individual species in their corresponding organonitrate groups.

Continuous  $\text{NH}_3$  concentrations were only measured during the last two intensives. Biweekly AMoN  $\text{NH}_3$  measurements, with corrections for travel blanks and atmospheric pressure, were used to establish a continuous 12-  
395 month time series of air concentration for annual deposition modeling. Ammonia concentrations are known to exhibit pronounced diel patterns, even in remote areas (Wentworth et al., 2016). Variability in air concentration interacts with diel cycles in surface wetness, turbulence, and other factors to influence diel patterns in air-surface exchange rates. To incorporate this interaction, the diel concentration pattern determined during spring and summer 2016 by MARGA  $\text{NH}_3$  measurements (Supplemental Figure S7) was imposed on the bi-weekly AMoN  $\text{NH}_3$  concentration. The hourly  
400 profile of  $\text{NH}_3$  concentrations was normalized by the corresponding overall mean concentration to produce a normalized mean diel concentration profile. This profile was then applied to each biweekly AMoN air concentration, temporally scaling the  $\text{NH}_3$  concentration by time of day while maintaining the measured biweekly AMoN concentration. Gap filling of AMoN data was not required. Comparisons of  $\text{NH}_3$  measurements are briefly discussed in Supplemental Section S1.

405 Hi-Vol measurements of speciated particulate N were only conducted during intensive periods to assess the relative contributions of inorganic and organic fractions to total water-soluble N. The CASTNET particulate  $\text{NH}_4^+$  and  $\text{NO}_3^-$  were used to provide a continuous 12-month time series of air concentration for annual deposition modeling. Concentrations of Hi-Vol and CASTNET measurements were shown to be comparable (Supplemental Section S1). For the annual time series, particulate organic nitrogen (PON) concentration was estimated based on speciated  
410 measurements during intensives, which showed that inorganic N accounts for ~88% of WSTN on average. Weekly average PON concentration was estimated from the weekly CASTNET measurements assuming  $\text{NH}_4^+ + \text{NO}_3^-$  represents 88% of total particulate nitrogen and PON represents the balance (12%). Weekly concentrations were then expressed at the hourly time scale for modeling. Gap filling of CASTNET data was not required.



415 Components of the atmospheric reactive N budget that are not routinely measured at Coweeta and were not directly  
measured during SANDS include NO, NO<sub>2</sub>, HONO, and N<sub>2</sub>O<sub>5</sub>. At the continental scale, regional model simulations  
suggest that NO, HONO and N<sub>2</sub>O<sub>5</sub> make minor contributions to the total dry deposition of reactive N (~ 2%), though  
the contribution of NO<sub>2</sub> is larger (~ 6%) (Walker et al., 2020). While NO, HONO, and N<sub>2</sub>O<sub>5</sub> have been excluded from  
our modeling analysis, we have included an estimate of NO<sub>2</sub> concentration, from which dry deposition is estimated,  
based on measured NO<sub>y</sub> and CMAQ (V5.2.1) derived estimates of the ratio of NO<sub>2</sub> to NO<sub>y</sub> at Coweeta. The “other”  
420 fraction of NO<sub>y</sub> (i.e., NO<sub>y</sub> – HNO<sub>3</sub> – ΣPN – ΣAN) measured at Coweeta represents between 47% (summer) and 76%  
(winter) of total NO<sub>y</sub> on a seasonal basis. This “other” fraction includes NO, NO<sub>2</sub>, HONO, N<sub>2</sub>O<sub>5</sub>, and some NO<sub>3</sub><sup>-</sup> but  
is likely dominated by NO<sub>2</sub>. The measured diel profile of “other” NO<sub>y</sub> (Supplemental Figure S8) concentration shows  
the typical pattern indicative of morning and evening modes related to mobile NO<sub>x</sub> emissions. Winds at Coweeta are  
from the east/northeast during the morning, which is the direction of local residences, the town of Otto, NC, and U.S.  
425 Highway 23. Winds are from the west/southwest during the evening, which is the direction of the Nantahala National  
Forest. Consistent with the diel profile of “other” NO<sub>y</sub>, a much larger morning peak in NO<sub>2</sub> is therefore expected. To  
estimate the concentration of NO<sub>2</sub> from the measured “other” NO<sub>y</sub>, we examined the ratio of NO<sub>2</sub> to the quantity NO<sub>y</sub>  
– HNO<sub>3</sub> – PANS – NTR (e.g., “other” NO<sub>y</sub>) simulated by CMAQ (V5.2.1) for the Coweeta site over the year 2015,  
where PANS represents total peroxy nitrates, and NTR represents other organic nitrates. Relative to the measured  
430 NO<sub>y</sub> species, PANS and NTR are assumed to represent ΣPN and ΣAN, respectively. The ratio of CMAQ estimated  
NO<sub>2</sub> to “other” NO<sub>y</sub> ranges from 0.51 during summer to 0.60 during winter. These seasonal factors were applied to  
the measured “other” NO<sub>y</sub> to estimate the hourly NO<sub>2</sub> concentration. Gap filling procedures for hourly “other” NO<sub>y</sub>  
follow those for HNO<sub>3</sub>, ΣPN, and ΣAN described above. Details of CMAQ V5.2.1 can be found in Supplemental  
Table S3.

### 3 Results and discussion

#### 435 3.1 Long-term trends in atmospheric N at Coweeta

Emissions of oxidized nitrogen (NO<sub>x</sub>) and sulfur (SO<sub>x</sub>) have declined significantly in the eastern U.S. in response to  
the 1990 Clean Air Act Amendments (Figure 2, Supplemental Figure S9). Trends data from U.S. EPA’s National  
Emissions Inventory (NEI) indicate a nationwide decline of 74% and 46% for SO<sub>x</sub> and NO<sub>x</sub> emissions from the early  
1990s to 2010s, respectively, comparing 1990–1994 to 2010–2014 annual averages (U.S. EPA, 2014). By contrast,  
440 NH<sub>3</sub> emissions have been reported as relatively unchanged or slightly increasing for the same periods (Ellis et al.,  
2013; Paulot and Jacob, 2013; Xing et al., 2013), depending on the location and region of the U.S. Declining NO<sub>x</sub> and  
SO<sub>x</sub> emissions have resulted in decreasing trends in air concentrations of HNO<sub>3</sub> and SO<sub>2</sub> at Coweeta between the 1990s  
and 2010s (Figures 2 and S9). Concentrations noticeably began to decline in 2008, the timeline of which likely  
indicates the effect of full implementation of the 2006 Tier 2 Gasoline Sulfur Program, as well as the enactment of the  
445 Clean Air Interstate Rule (CAIR), both of which aimed to further reduce NO<sub>x</sub> and SO<sub>x</sub> emissions (Sickles and



Shadwick, 2015; LaCount et al., 2021). Compared to other species,  $\text{NH}_3$  concentrations have only been measured at Coweeta for a relatively short period of time.

Atmospheric  $\text{NH}_3$  reacts with acidic sulfate to form ammonium sulfate ( $(\text{NH}_4)_2\text{SO}_4$ ) or bi-sulfate ( $(\text{NH}_4)\text{HSO}_4$ ) aerosol. Under favorable thermodynamic conditions (low temperature and high RH),  $\text{NH}_3$  in excess of acidic sulfate will react with  $\text{HNO}_3$  to form ammonium nitrate aerosol ( $\text{NH}_4\text{NO}_3$ ). Concentrations of  $\text{SO}_4^{2-}$  at Coweeta have tracked  $\text{SO}_2$ , and subsequently,  $\text{NH}_4^+$  concentrations have declined substantially relative to early 1990s levels (Figure 2). However, concentrations of  $\text{NO}_3^-$  aerosol, which are relatively low at Coweeta, have not followed trends in  $\text{SO}_4^{2-}$  and  $\text{NH}_4^+$  (Figure 2). Previous studies at other U.S. sites have also reported non-proportional changes in  $\text{PM}_{2.5}$  mass in response to  $\text{SO}_2$  and  $\text{NO}_x$  control strategies (Blanchard and Hidy, 2005; Sickles and Shadwick, 2015). Non-linear reductions or increases of particulate  $\text{NO}_3^-$  with coincident  $\text{SO}_2$  and  $\text{NO}_x$  emission reductions relate to the thermodynamic equilibrium of the  $\text{SO}_4^{2-}$ - $\text{NO}_3^-$ - $\text{NH}_4^+$ - $\text{HNO}_3$ - $\text{NH}_3$  aerosol system. As ambient  $\text{SO}_4^{2-}$  concentrations decline, the capacity for  $\text{NH}_4^+$  formation (i.e., neutralization) also decreases, leaving additional  $\text{NH}_3$  in the gas phase. Amounts of  $\text{NH}_3$  in excess of acidic  $\text{SO}_4^{2-}$  can subsequently react with  $\text{HNO}_3$  to form  $\text{NH}_4\text{NO}_3$ , confounding the relationship between  $\text{NO}_x$  emission reductions and atmospheric  $\text{NO}_3^-$  concentrations.

The long-term trend in  $\text{NO}_3^-$  wet deposition at Coweeta (Figure 3) has tracked the downward trend in ambient  $\text{HNO}_3$  concentration. Wet deposition of  $\text{NH}_4^+$ , however, shows no apparent trend, in contrast to the decline in  $\text{NH}_4^+$  aerosol concentration. This pattern may relate to the combined effects of changes in regional  $\text{NH}_3$  emissions, aerosol chemistry, and dry deposition rates on the long-term trend in atmospheric  $\text{NH}_3$  concentrations. As noted above, declines in  $\text{SO}_2$  emissions and  $\text{SO}_4^{2-}$  aerosol result in less conversion of  $\text{NH}_3$  to  $\text{NH}_4^+$  aerosol, leaving more  $\text{NH}_3$  in the gas phase. Furthermore, reduced air concentrations of acidic species such as  $\text{SO}_2$  and  $\text{HNO}_3$  result in lower dry deposition rates and subsequently less acidic deposition surfaces, which in turn reduces the deposition velocity (i.e., increases the atmospheric lifetime) of  $\text{NH}_3$  (Sutton et al., 2003). In addition to changes in emissions, these two processes are thought to be at least partly responsible for the increases in  $\text{NH}_3$  air concentrations that have been observed in some locations across the U.S. (Butler et al., 2015; Yu et al., 2018; Yao and Zhang, 2019). While there is no discernable trend in  $\text{NH}_3$  air concentrations over the relatively short period of record at Coweeta, a decline in wet deposition of  $\text{NH}_4^+$  aerosol may have been offset to some extent by increased wet deposition of  $\text{NH}_3$  gas (Asman et al., 1995), which is highly soluble, resulting in an overall lack of trend in  $\text{NH}_4^+$  wet deposition at Coweeta over time. Similar to other areas in the U.S. (Li et al., 2016), the downward trend in  $\text{NO}_3^-$  wet deposition has led to an increase in the relative contribution of reduced forms of N (i.e.,  $\text{NH}_x = \text{NH}_3 + \text{NH}_4^+$ ) to inorganic wet N deposition at Coweeta ( $\text{NH}_4^+:\text{NO}_3^-$ , Figure 3).

### 3.2 Wet deposition

Of the various forms of N in precipitation, ammonium was the most abundant inorganic species, contributing 47.0% of WSTN in weekly samples ( $N = 52$ ), on average, followed by  $\text{NO}_3^-$  (41.7%, Figure 4, Supplemental Table S4). The contribution of  $\text{NO}_2^-$  was negligible. Organic compounds (WSON) contributed 11% of WSTN, on average, which is within the range of values (3% to 33%) reported for other locations in the U.S. (Scudlark et al., 1998; Whittall and Paerl, 2001; Keene et al., 2002; Beem et al., 2010; Walker et al., 2012; Benedict et al., 2013). While concentrations



of N compounds were generally higher during warm months, a seasonal pattern in the percent contribution of WSON to WSTN was not apparent. In a previous study at Coweeta (1994–1996), Knoepp et al. (2008) found that organic nitrogen contributed 21% of total nitrogen in bulk (wet + dry) deposition samples. Differences between Knoepp et al. 485 (2008) and SANDS results may be related to interannual variability or trends in rainfall composition over the intervening two decades (e.g., Figure 3) or differences in collection method (wet only versus bulk deposition) or analytical techniques used for total N analysis (persulfate/UV digestion (Walker et al., 2012) versus total Kjeldahl N (Knoepp et al., 2008)).

### 3.3 Air concentrations of oxidized N

490 The oxidized fraction of reactive nitrogen (NO<sub>y</sub>) comprises a mixture of gaseous and particulate inorganic (NO, NO<sub>2</sub>, N<sub>2</sub>O<sub>5</sub>, HONO, HNO<sub>3</sub>, NO<sub>3</sub><sup>-</sup>) and organic compounds. Owing to its large deposition velocity and typical atmospheric concentration, HNO<sub>3</sub> is the primary contributor to dry deposition of inorganic oxidized N (Walker et al., 2020). Much less is known about the dry deposition of oxidized organic nitrogen compounds (Walker et al., 2020). Peroxy nitrates (PNs) and alkyl and multifunctional nitrates (ANs) are formed during the photochemical oxidation of volatile organic 495 compounds (VOCs) in the presence of NO<sub>x</sub> (NO<sub>x</sub> = NO + NO<sub>2</sub>). While PNs exist in the gas phase, ANs can exist in the gas or particle phase and can be the dominant chemical sink for NO<sub>x</sub> in high biogenic VOC (BVOC)/low NO<sub>x</sub> environments (Farmer et al., 2008; Browne and Cohen, 2012; Paulot et al., 2012; Browne et al., 2013). Unlike PNs, ANs can also form at night via nitrate radical-induced oxidation of VOC. Further, PNs and ANs have been shown to contribute significantly to the total NO<sub>y</sub> budget in geographically diverse rural and forested environments (e.g., Trainer et al., 1993; Nouaime et al., 1998; Farmer et al., 2008; Browne et al., 2013; Toma et al., 2019). Flux measurements at 500 Blodgett Forest, CA, showed that PN dry deposition contributed 4–19% of total N deposition at the site (Wolfe et al., 2009). Chemical transport modeling with current representation of the atmospheric oxidized nitrogen system suggests that PNs and ANs together contribute ~ 6% of total N deposition and ~ 12% of dry N deposition at the U.S. continental scale, compared to ~ 21% and 34% for HNO<sub>3</sub> and ~ 6% and 9% for particulate NO<sub>3</sub><sup>-</sup> (Walker et al., 2020).

505 The annual average concentration of NO<sub>y</sub> was 1.00 ppb, with the highest seasonal average concentration in the winter (1.32 ppb) and lowest in the summer (0.64 ppb) (Figure 5, Table S5). The nearest rural NO<sub>y</sub> monitoring site is 85 km to the northwest at Look Rock in the Great Smoky Mountains National Park, where the annual concentration was 1.5 ppb over the same period (NPS, 2020). Similar to Coweeta, NO<sub>y</sub> concentrations at Look Rock are typically lowest during summer and highest in winter, though the seasonal cycle exhibits some interannual variability. The annual 510 mean concentrations of HNO<sub>3</sub>, ΣPN, ΣAN determined by TD-PC-CL were 0.14, 0.1, and 0.09 ppb, respectively (Figure 5). HNO<sub>3</sub> and ΣPN concentrations peaked in spring, coincident with the seasonal peak in O<sub>3</sub> concentration, while concentrations of ΣAN were similar in spring and summer. Diel patterns of HNO<sub>3</sub>, ΣPN, and ΣAN peaked during the day as expected for photochemical products. However, of the organic compounds, the ratio of peak daytime to minimum nighttime concentrations (Figure 5) was much smaller for ΣAN (2.3) compared to ΣPN (3.9), possibly 515 indicative of the additional nighttime formation of AN.

Annually, HNO<sub>3</sub> (12.8%), ΣPN (12.2%), and ΣAN (12.7%) contributed approximately the same proportions of the NO<sub>y</sub> budget (Figure 5, Table S6). Their collective contribution (NO<sub>z</sub> = HNO<sub>3</sub> + ΣPN + ΣAN) to total NO<sub>y</sub> peaked



during the summer (52.9%) and reached a minimum during winter (24.2%). The contributions of  $\Sigma$ PN (16.7%) and  $\Sigma$ AN (20.0%) exceeded  $\text{HNO}_3$  (16.2%) during summer when total NOy concentrations were lowest. Our results fall  
520 within the range of NOy budgets reported for other rural forested sites, in which  $\Sigma$ PN and  $\Sigma$ AN contribute  $\sim 8$ –40% (Nouaime et al., 1998; Farmer et al., 2008; Browne et al., 2013; Toma et al., 2019) and 10–22% (Day et al., 2003; Farmer et al., 2008; Browne et al., 2013) of NOy, respectively.

To put the SANDS period into context with longer-term variability of oxidized N concentrations at Coweeta, CASTNET  $\text{HNO}_3$  and  $\text{NO}_3^-$  measurements for the period 2015–2020 are summarized in Figure 6 along with the  
525 SANDS period. We note here that  $\text{NH}_4\text{NO}_3$  volatility on the CASTNET Teflon filter can result in positive and negative biases in  $\text{HNO}_3$  and  $\text{NO}_3^-$ , respectively, with larger biases expected under warmer conditions (Lavery et al., 2009). Studies have shown the total  $\text{NO}_3^-$  ( $\text{TNO}_3 = \text{HNO}_3$  and  $\text{NO}_3^-$ ) to be conserved, though some portion of the  $\text{NO}_3^-$  collected by the CASTNET open-faced filter may be contributed by coarse particles. The partitioning of  $\text{TNO}_3$  between gas and particulate phases is important, given the much larger deposition velocity of  $\text{HNO}_3$  than  $\text{NO}_3^-$ . The  
530 CASTNET measurements reflect relatively low concentrations of both  $\text{HNO}_3$  and  $\text{NO}_3^-$ , with  $\text{HNO}_3$  exceeding  $\text{NO}_3^-$  during all seasons. Particulate  $\text{NO}_3^-$  concentrations are highest during cooler months, as expected, and negligible during the summer, a pattern that is consistent with observations from other networks across the Southeast (Kim et al., 2015). Additionally,  $\text{TNO}_3$  is primarily in the gas phase even during winter. Seasonal mean concentrations during the SANDS period fall within the interquartile range (IQR) of the 6-year period between 2015 and 2020, with SANDS  
535 annual and 6-year averages being very similar (Figure 6). Seasonal and annual mean  $\text{HNO}_3$  concentrations agreed closely with the CASTNET measurements (Figures 6 and Supplemental Section S1).

### 3.4 Air concentrations of reduced N

Reduced forms of nitrogen ( $\text{NH}_x$ ) represent another important component of the inorganic dry N deposition budget. At the continental scale,  $\text{NH}_3$  dry deposition contributes  $\sim 20\%$  of total N deposition and  $\sim 32\%$  of dry N deposition,  
540 whereas the contributions from  $\text{NH}_4^+$  aerosol are  $\sim 4\%$  and  $\sim 6\%$ , respectively (Walker et al., 2020). Similar to oxidized forms of N, the partitioning of mass between the gas ( $\text{NH}_3$ ) and particulate ( $\text{NH}_4^+$ ) phases affects the dry deposition rate of  $\text{NH}_x$ , given the larger deposition velocity of  $\text{NH}_3$  relative to  $\text{NH}_4^+$ .

During 2015–2020, with 2020 being the most recent full year of AMoN data, concentrations of  $\text{NH}_3$  and  $\text{NH}_4^+$  were similar, though with slightly more mass in the particulate phase (53.8%, Figure 7). Both species displayed a seasonal  
545 pattern of lowest concentrations in the winter and higher concentrations during warm months.  $\text{NH}_3$  concentrations peaked in summer, reflecting the temperature dependence of regional agricultural and biogenic emissions.  $\text{NH}_4^+$  concentrations followed the seasonal cycle in  $\text{SO}_4^{2-}$  concentrations, which were also similar in spring and summer and minimum in winter at Coweeta. The seasonal cycle of  $\text{NH}_3/\text{NH}_4^+$  partitioning was driven more by  $\text{NH}_3$  than  $\text{NH}_4^+$ , the former exhibiting more seasonal variability. Hourly measurements conducted during spring and summer 2016 showed  
550 that  $\text{NH}_3$  also displayed significant diel variability (Supplemental Figure S7), reaching a maximum around mid-day and minimum overnight. Seasonal mean concentrations during the SANDS period fall within the IQR of the 6-year period between 2015 and 2020, with SANDS annual and 6-year averages being very similar. Concentrations of  $\text{NH}_x$  were higher relative to  $\text{TNO}_3$  during SANDS and over the longer term at Coweeta (Figures 6 and 7).





### 3.5 Aerosol N composition

555 Ammonium was the most abundant inorganic species, contributing 86.8% of WSTN ( $N = 103$ ) on average (Figure 8, Table S7). The contributions of  $\text{NO}_3^-$  and  $\text{NO}_2^-$  were negligible. Organic compounds (WSON) contributed 11.6% of WSTN, which is very similar to precipitation. Our study-wide average of %WSON is slightly lower than measurements at other North American forest sites, including Duke Forest, North Carolina (~33%, Lin et al., 2010) and Rocky Mountain National Park (14–21%) (Benedict et al., 2012), but is within the global range of 10–39% (Cape  
560 et al., 2011). Similar to precipitation chemistry, there was no seasonal pattern in the percent contribution of WSON to WSTN in  $\text{PM}_{2.5}$ . Hi-Vol measurements of inorganic PM components compared well, overall, with collocated CASTNET measurements (Supplemental Section S1).

### 3.6 Biogeochemistry

Estimates of  $\text{NH}_3$  emission potentials ( $\Gamma$ ) for the ground and vegetation are needed to calculate compensation points  
565 ( $\chi$ ) and fluxes in STAGE. Measurements of pH,  $\text{NH}_4^+$  and corresponding  $\Gamma$  of the leaves ( $\Gamma_s$ ) and litter ( $\Gamma_l$ ) are summarized in Figure 9 and Supplemental Tables S8 and S9. Measurements of  $\Gamma_s$  are divided into green leaves collected during the growing season (spring and summer) and senescent leaves collected in October.  $\text{NH}_3$  emission potentials ( $\Gamma$ ) for green leaves ( $\Gamma_s$ ) ranged from zero to 4070 with a median value (35.8) (Table S8) corresponding to a compensation point of  $\chi_s = 0.25 \mu\text{g NH}_3 \text{ m}^{-3}$  at 25 °C. Large intra-species variability of tissue pH and  $\text{NH}_4^+$  were  
570 observed (Table S9) and separating by crown versus understory species did not reveal distinct differences between groups. Given the variability of the observations, the median  $\Gamma_s$  was used for STAGE simulations. Senescence marks the translocation of N in leaves to storage tissues (Schneider et al., 1996). Along with a decline in photosynthetic activity, degradation of chlorophyll, and other metabolic changes, glutamine synthetase (GS) activity also declines (Pearson et al., 2002). Glutamine synthetase catalyzes assimilation of  $\text{NH}_4^+$  into glutamine and is therefore important  
575 in regulating the pool of  $\text{NH}_4^+$  available for exchange as  $\text{NH}_3$  between the leaf and atmosphere and remobilizing organic N for storage during senescence. A decline in GS activity can thus result in increased leaf  $\text{NH}_4^+$  concentrations (Pearson et al., 2002; Wang et al., 2011). Senescent leaves were similar to green leaves with respect to median tissue pH but showed distinctly higher concentrations of tissue  $\text{NH}_4^+$ . Median  $\Gamma_s$  was correspondingly higher (113), equivalent to  $\chi_s = 0.8 \mu\text{g NH}_3 \text{ m}^{-3}$  at 25 °C. For STAGE modeling, the median  $\Gamma$  for senescent leaves was used for  $\Gamma_s$   
580 during the fall.

Leaf litter on the soil surface has been shown to be a source of  $\text{NH}_3$  to the atmosphere in both natural and agricultural ecosystems (Nemitz et al., 2000b; David et al., 2009; Hansen et al., 2013). As litter decomposes, mineralization of organic N is a source of  $\text{NH}_4^+$ , some of which is lost to the overlying air as  $\text{NH}_3$ . Litter  $\text{NH}_4^+$  concentrations were similar to green leaves but lower than senescent leaves (Figure 9). However, the pH was higher than both green and  
585 senescent leaves. The resulting median  $\Gamma_l$  (69.3) was larger than green leaves but smaller than senescent leaves, equivalent to  $\chi_l = 0.49 \mu\text{g NH}_3 \text{ m}^{-3}$  at 25 °C. Litter  $\Gamma$  was much larger than that of the underlying soil. Average (0–10 cm soil depth) soil pH (4.18) and  $\text{NH}_4^+$  ( $1.21 \text{ mg N kg}^{-1}$ ) correspond to  $\Gamma_{\text{soil}} = 10$  at a soil mass wetness of  $0.1 \text{ g g}^{-1}$ , equivalent to  $\chi_{\text{soil}} = 0.07 \mu\text{g NH}_3 \text{ m}^{-3}$  at 25 °C. This very low  $\Gamma_{\text{soil}}$  results from the low pH of the shallow soil.



Vertical profiles of air concentrations within and above the canopy were measured to investigate patterns of air-surface exchange with specific ecosystem compartments (i.e., canopy crown, understory, and ground). A detailed analysis of bi-directional N fluxes is forthcoming; thus, we limit the discussion of these data to  $\text{NH}_3$  in the context of interpreting patterns observed in the biogeochemical emission potentials and their prescription in the STAGE model. Nitric acid,  $\text{NH}_4^+$ , and  $\text{NO}_3^-$  showed expected decreasing concentrations from above the canopy to the forest floor, indicative of deposition. While  $\text{NH}_3$  profiles showed patterns of deposition to the crown and understory, concentrations near the forest floor indicated both emissions and deposition (Figure 10). Of the 76 daytime profiles measured, 40% showed decreases toward the forest floor, and 60% showed increasing concentration from approximately the lower understory (~ 5 m above ground) to the forest floor. The former pattern is interpreted as deposition to the forest floor, and the latter is interpreted as emission. Thus, the mean profile suggests a source of  $\text{NH}_3$  at the ground. The very low  $\Gamma_{\text{soil}}$  suggests that emission from the soil is unlikely given such a low pH. The leaf litter layer, which indicates a much higher emission potential ( $\Gamma_1$ ) than the soil, is a more likely source of  $\text{NH}_3$ . This hypothesis is consistent with Hansen et al. (2013; 2017), in which emissions of  $\text{NH}_3$  from a beech (*Fagus sylvatica*) forest after leaf fall were attributed to the decomposition of new litter. Similar to our site, the underlying soil also had low pH (4–5). Given our observations, we used  $\Gamma_1$  (median = 69.3, Table S8) rather than  $\Gamma_{\text{soil}}$  as the ground emission potential ( $\Gamma_g$ ) in STAGE.

### 3.7 N deposition budget

Total annual N deposition for the period August 2015 – August 2016 was 6.6 kg N ha<sup>-1</sup> (Figure 11). Over this period, wet deposition contributed 61.4% of total N deposition, of which  $\text{NH}_4^+$  was the primary component (29.9%). Wet deposition of organic N contributed 5.5% of the total N deposition budget. Dry deposition accounted for 38.7% of total deposition, of which  $\text{NH}_3$  was the primary contributor (19.7%). Reduced forms of inorganic N were the largest contributor to the budget (50.7%), with oxidized inorganic and organic N contributing 41.6% and 7.7% of total N deposition, respectively. Dry deposition of organic N made a small contribution (2.2%) to the total deposition budget. Ammonia is the most important contributor to the dry deposition budget (51%) and differs from the other species in that it is exchanged bidirectionally between the ground, canopy and atmosphere. Seasonal net canopy-scale and component fluxes are shown in Supplemental Figure S10. The mean net flux ( $F_{\text{net}}$ ) is downward (i.e., deposition) during all seasons, generally following the seasonal pattern of the atmospheric  $\text{NH}_3$  concentration. The cuticular flux ( $F_{\text{cut}}$ ), which is unidirectional in STAGE, is the dominant deposition pathway, and ranged from -89.0 ng N m<sup>-2</sup> s<sup>-1</sup> (deposition) to near zero, and accounted for 72%, 81%, 96%, and 98% of the net flux in winter, spring, summer and fall, respectively. The stomatal flux ( $F_s$ ) is bidirectional, ranging from -4.2 ng N m<sup>-2</sup> s<sup>-1</sup> (deposition) to 2.4 ng N m<sup>-2</sup> s<sup>-1</sup> (emission), with the largest fluxes occurring during warmer periods of the growing season when the stomatal resistance is lowest. Low LAI and large stomatal resistance in winter and fall and offsetting bidirectional fluxes in spring and summer result in a relatively small mean stomatal deposition flux ( $F_s$ ) across seasons. On an annual scale, the ground flux ( $F_g$ ) makes a larger contribution (7.2%) than  $F_s$  (2.4%) to  $F_{\text{net}}$ .  $F_g$  is also bidirectional, ranging from -4.3 ng N m<sup>-2</sup> s<sup>-1</sup> (deposition) to 0.4 ng N m<sup>-2</sup> s<sup>-1</sup> (emission). Fluxes are largest during spring as atmospheric  $\text{NH}_3$  begins to increase with warmer temperatures but before peak LAI is reached, after which the denser canopy increases



the in-canopy aerodynamic ( $R_{mc}$ ) and air-side ground boundary-layer resistances ( $R_{bg}$ ) (Table S2), thereby decreasing  
625  $F_g$ .  
Nitric acid was the second largest component of dry deposition, contributing 37.1% of the total. While  $\text{HNO}_3$  deposits  
more rapidly than  $\text{NH}_3$  (Supplemental Table S10), the overall importance to the dry N budget is constrained by  
relatively low air concentrations at this remote forest site ( $< 0.2$  ppb on average). Particulate species made much  
smaller contributions to the budget due to much lower deposition velocities ( $V_d = \text{flux}/\text{air concentration}$ ) relative to  
630 their gaseous counterparts (Supplemental Table S10). For example, while  $\text{NH}_4^+$  contributed more to the  $\text{NH}_x$   
concentration budget than  $\text{NH}_3$ , (Figure 7), the  $\text{NH}_x$  flux budget was regulated by the much more rapid exchange of  
 $\text{NH}_3$  between the forest and atmosphere relative to  $\text{NH}_4^+$ . A similar example was observed for oxidized N. While  $\text{NO}_2$   
represents an important fraction of the oxidized N concentration budget via its contribution to “Other  $\text{NO}_y$ ”,  $\text{NO}_2$   
deposits much less rapidly than  $\text{HNO}_3$  (Supplemental Table S10) thereby contributing a relatively small fraction  
635 (3.1%) of the dry N flux. Of the organic N species, AN contributed slightly more (3.0%) to dry N deposition than PN  
(2.3%) owing to a higher deposition velocity (Supplemental Table S10). Similar to particulate  $\text{NH}_4^+$  and  $\text{NO}_3^-$ , PON  
made a small contribution to dry N deposition (0.4%) due to its low  $V_d$  (Supplemental Table S10). Reduced forms of  
N accounted for the majority of dry N deposition (53.9%), with oxidized inorganic and organic forms of N contributing  
40.5% and 5.7%, respectively.  
640 Total N deposition peaked during the summer ( $2.5 \text{ kg N ha}^{-1}$ ) and reached a minimum in the fall ( $1.0 \text{ kg N ha}^{-1}$ ) (Figure  
12). Wet deposition exceeded dry deposition during all seasons. Seasonal variability in wet deposition was primarily  
driven by precipitation amount, whereas dry deposition was influenced by seasonality in air concentrations of the  
primary  $\text{N}_r$  species (Figures 6 and 7) and leaf area index (Figure S6). Ammonia fluxes followed the seasonal pattern  
of air concentration, peaking in the summer and reaching a minimum in winter. Concentrations and fluxes of  $\text{HNO}_3$   
645 peaked in the spring and reached a minimum in the fall. Deposition velocities, which can be thought of as the  
concentration-normalized flux, peaked during the summer and reached a minimum during winter for most N species.  
This pattern largely reflects the seasonal cycle in leaf area index, i.e., the total surface area of the forest canopy  
available for dry deposition. The seasonal pattern of  $V_d$  for  $\text{HNO}_3$  differed slightly from the other species, peaking in  
spring and reaching a minimum in fall. In contrast to other N species,  $\text{HNO}_3$  deposition is limited by turbulent transfer,  
650 the canopy (surface) resistance being zero. The pattern of  $\text{HNO}_3$   $V_d$  thus partially reflects seasonal patterns in wind  
speed and degree of turbulent mixing above the canopy.

### 3.8 Evaluation of the dry deposition model

While total uncertainty in the dry deposition budget cannot be rigorously quantified (Walker et al., 2019a), the  
sensitivity of the model to parameterizations and key inputs can elucidate important aspects of model uncertainty and  
655 inform a potential range of dry deposition estimates. Here we undertake such an exercise, evaluating several alternative  
modeling scenarios to assess the sensitivity of fluxes and total dry deposition to assumptions regarding LAI,  $\text{NH}_3$   
emission potentials ( $\Gamma_{s,i}$ ),  $\text{NH}_3$  cuticular resistance ( $R_{cut,dry}$ ), and particle size distribution. We focus on  $\text{NH}_3$ , as it is  
the most important component of the dry deposition budget and more complex with regard to air-surface exchange  
processes than the other species. Sensitivity tests are summarized in Supplemental Section S5 and Table S11. Of the



660 scenarios tested, increasing  $\Gamma_1$  and  $\Gamma_s$  within the range of observations and reducing  $R_{cut,dry}$  within the variability reported by Massad et al. (2010) exerted the largest control over the dry deposition flux, establishing a range of total dry deposition from 2.1 (increasing  $\Gamma_{s,1}$ ) to 3.0 (decreasing  $R_{cut,dry}$ )  $\text{kg N ha}^{-1}$  around the base value of 2.6  $\text{kg N ha}^{-1}$ . The corresponding % contribution of  $\text{NH}_3$  to total dry N deposition ranges from 40.6% to 57.1% (base = 51%) and the contribution of dry to total wet + dry deposition ranges from 34.4% to 42.1% (base = 38.7%). Our results point to

665 the need for a better understanding of the processes of cuticular exchange and the importance of adequately characterizing the magnitude and variability of vegetation and litter emission potentials in forests.

Another method of evaluating model behavior is the comparison with measured  $V_d$ . During the final summer intensive, a small dataset ( $N = 19$  observations) of  $V_d$  was determined from daytime measurements of vertical concentration gradients above the canopy using the MBR method. Measured  $V_d$  was compared to  $V_d$  derived from the STAGE model

670 for overlapping periods, and the maximum possible  $V_{dmax}$  as  $1/(R_a + R_p)$ . Of the 19 MBR measurements, four  $\text{NH}_3$  profiles exhibited emissions (6.8 to 22.4  $\text{ng NH}_3 \text{ m}^2 \text{ s}^{-1}$ ), which were not reproduced by STAGE. Analysis of the meteorological conditions during the MBR measurements suggests that emissions tend to occur during the warmest periods with lowest relative humidity. This would correspond to periods when  $R_{cut}$  and  $X_s$  are high and may indicate that the model is underestimating  $F_s$  emissions during these periods. Excluding the four emission periods,  $V_d$  estimated

675 from MBR and STAGE agree reasonably well (Supplemental Figure S12). As is the case for STAGE, resistance-based models typically assume  $\text{HNO}_3$  deposits at the rate of  $V_{dmax}$  (i.e.,  $R_c = 0$ ). As shown in Figure S12, fluxes measured during summer 2016 showed MBR  $V_d$  for  $\text{HNO}_3$  larger than  $\text{NH}_3$ , as expected, but lower than  $V_{dmax}$ . This apparent non-zero  $R_c$  could result from a real non-zero  $R_c$  caused, for example, by equilibrium of  $\text{HNO}_3$  and  $\text{NO}_3^-$  on leaf surfaces (Nemitz et al., 2004a). This pattern may also reflect the influence of flux divergence related to  $\text{NH}_4\text{NO}_3$

680 evaporation in the canopy crown, which would reduce the magnitude of the downward vertical gradients, and therefore the measured  $V_d$  of  $\text{HNO}_3$  and  $\text{NH}_3$  (Nemitz et al., 2004b). In this study, concentrations of  $\text{NO}_3^-$  (mean = 0.08  $\mu\text{g m}^{-3}$ ) were much lower than  $\text{HNO}_3$  (mean = 0.47  $\mu\text{g m}^{-3}$ ), and  $\text{NO}_3^-$  gradients were therefore difficult to resolve, precluding a definitive explanation of  $\text{HNO}_3$   $V_d < V_{dmax}$ . Ignoring potentially significant uncertainties related to the measurement of chemical and temperature gradients within the roughness sublayer, our results suggest that periods of  $\text{NH}_3$  emission

685 during the day, particularly at higher air temperature and lower humidity, may be underestimated. Our results also reinforce the need for temporally extensive measurements of concentrations and fluxes of  $\text{HNO}_3$ ,  $\text{NH}_3$ , and  $\text{NO}_3^-$  to examine exchange processes and uncertainties related to chemical flux divergence.

### 3.9 Spatial and temporal representativeness of deposition budget

The complexity of atmospheric flows in mountainous terrain influences the spatial variability of wet and dry deposition processes (Lehner and Rotach, 2018). As the deposition budget presented above is based on measurements

690 from the lowest elevation portion of the Coweeta basin, the degree to which the budget is spatially representative must be considered. Potential effects on dry deposition were assessed by characterizing the magnitude and spatial variability of  $\text{HNO}_3$  and  $\text{NH}_3$  concentrations along an elevation gradient (Figure 1, Table 1) from the lower to upper portions of the Coweeta Basin. It should be noted that  $\text{HNO}_3$  concentrations at NC25 were measured by CASTNET

695 while  $\text{HNO}_3$  passive samplers were used at the other locations. Concentrations are summarized in Figure 13, in which



the sites are ordered left to right from lowest to highest elevation. Analysis of variance (ANOVA) rank analysis indicated that the differences in  $\text{NH}_3$  across sites are statistically insignificant ( $p = 0.231$ ). For  $\text{HNO}_3$ , site differences were statistically significant ( $p = 0.008$ ) but primarily due to higher concentrations at a single site, Screwdriver Knob (SK). Screwdriver Knob is distinct from the other sites in that the measurement tower was situated on a relatively narrow exposed ridge. The measurements are therefore higher above the surrounding vegetation than at the other sites. With SK removed, differences among the other sites are statistically insignificant ( $p = 0.242$ ). Overall, variability across sites, even including SK, is sufficiently small such that spatial variability of dry deposition across the basin would likely be driven more by variability in meteorology than air concentrations.

A quantitative assessment of the effects of air flow on dry deposition across the basin is not possible, but the analysis of Hicks (2008) illustrates the relevant effects in the context of the resistance analogy for  $V_d$ . Over flat homogeneous terrain, flux to the vegetation is driven by turbulent diffusion in the vertical direction above the canopy and horizontal advection is assumed to be zero. In the extreme case of air flow approaching a steep forested slope, flux to the vegetation is driven by horizontal advection into the canopy, and the aerodynamic resistance ( $R_a$ ) becomes zero. Taking  $\text{HNO}_3$  as an example under the typical assumption that the canopy resistance ( $R_c$ ) = 0,  $V_d$  becomes limited by the quasi-laminar boundary layer resistance at the vegetation surfaces ( $R_b$ ). For the less extreme case of a uniformly vegetated gentle hill,  $V_d$  for  $\text{HNO}_3$  could be enhanced by a factor of  $[1+(R_a/R_b)]^{1/2}$  (Hicks, 2008). Using median values of  $R_a$  and  $R_b$  from our modeling period, this would increase  $V_d$  for  $\text{HNO}_3$  by a factor of  $\sim 1.3$ . For gases that have a significant  $R_c$ , enhancements will be smaller. Topographical relief across the Coweeta Basin may be gentle enough such that the flow separation described in the previous example is limited to certain areas and meteorological scenarios. However, as Hicks (2008) points out, flow complexity in mountainous areas has the overall effect of increasing  $V_d$ , with areal weighted fluxes being highly dependent on the topographical characteristics specific to the study area. Other effects related to katabatic flows (Novick et al., 2016) and diel patterns of hillside shading that drive temperature-related processes such as  $\text{NH}_3$  compensation points introduce additional uncertainties.

The results of Knoepp et al. (2008) show that spatial patterns of wet deposition across the Coweeta Basin follow patterns of precipitation amount, which increase with elevation. In their study, bulk deposition of  $\text{NH}_4^+$ ,  $\text{NO}_3^-$  and total organic nitrogen was measured from 1994–1996 at sites ranging in elevation from 788 to 1389 m. Annual precipitation depth and bulk deposition increased by 25% from the lowest to the highest elevation. This increase in precipitation with elevation is consistent with the 75-year analysis of Coweeta climatological data by Laseter et al. (2012), which showed annual precipitation amount at 1398 m was 32% greater than at 686 m. In our study, wet deposition was measured at the NC25 site at 686 m and therefore represents a lower wet deposition rate than would occur in higher elevation portions of the basin. An approximate 30% enhancement in both wet and dry (extreme case) deposition for the highest elevations within the basin would correspond to a total N deposition rate of  $8.6 \text{ kg N ha}^{-1} \text{ yr}^{-1}$  based on our estimate of  $6.6 \text{ kg N ha}^{-1} \text{ yr}^{-1}$  for the lower basin.

Regarding the temporal representativeness of the deposition budget calculated here, wet deposition of inorganic N ( $\text{NO}_3^- + \text{NH}_4^+$ ) during our 12-month model period ( $3.69 \text{ kg N ha}^{-1}$ ) agrees well with the mean annual deposition rate measured at NTN site NC25 ( $3.72 \text{ kg N ha}^{-1}$ ) over the period 2015–2020, with 2020 being the most recent full year of reported observations. Air concentrations of  $\text{NO}_3^-$  and  $\text{HNO}_3$  (Figure 6) as well as  $\text{NH}_3$  and  $\text{NH}_4^+$  (Figure 7) during



our model period are also similar to the 6-year (2015–2020) mean concentrations measured by CASTNET and AMoN. In this context, our results are deemed temporally representative of the most recently available complete years of monitoring data.

#### 4 Conclusions

Due to the success of the Clean Air Act, air concentrations and wet deposition of reactive N at Coweeta are the lowest observed since the beginning of routine monitoring in the late 1970s. However, even at historically low levels, our results show that  $N_r$  deposition remains highly ecologically relevant in the context of critical loads. Our estimate of total  $N_r$  deposition of  $6.6 \text{ kg N ha}^{-1} \text{ yr}^{-1}$  is near the upper-end estimate of mass balance derived critical loads ( $2.8$  to  $7$   $\text{kg N ha}^{-1} \text{ yr}^{-1}$ ) recently reported for spruce-fir, beech, and mixed deciduous forests by Pardo et al. (2018) in nearby Great Smoky Mountains National Park. Our result also falls within the range of empirical critical loads of N for combined tree health and biogeochemical responses ( $3$ – $8 \text{ kg N ha}^{-1} \text{ yr}^{-1}$ ) and changes in mycorrhizal fungi spore abundance, community structure and community composition ( $5$ – $12 \text{ kg N ha}^{-1} \text{ yr}^{-1}$ ) in eastern temperate forests (Pardo et al., 2011).

A key feature of the deposition budget derived for Coweeta is the predominance of reduced forms ( $\text{NH}_x$ ) of inorganic nitrogen (50.1%) over oxidized inorganic N (41.6%). Reductions in deposition of  $\text{NH}_x$  will be needed to achieve the lower-end estimates of critical N loads ( $\sim 3 \text{ kg N ha}^{-1} \text{ yr}^{-1}$ ) for southern Appalachian forests. This presents a challenge, as emissions and air concentrations of  $\text{NH}_3$  remain unregulated. Our results also show that organic forms of N make a non-trivial contribution (7.7%) to total N deposition, primarily via wet deposition. It is noted, however, that the gas-phase dry component of deposition only considers oxidized forms as alkyl and peroxy nitrates, excluding contributions from reduced (i.e., NH) organic compounds. While our results represent an advancement in accounting for organic dry  $N_r$  deposition in total  $N_r$  deposition, the application of new measurement technologies (Walker et al., 2019b) for broader chemical speciation of organic forms of dry  $N_r$  deposition is needed.

Our results underscore the need for long-term measurements of reactive chemical fluxes, and the coupling of atmospheric and biogeochemical measurements, to improve air-surface exchange models. Novel measurements that more directly elucidate the role of cuticular exchange of  $\text{NH}_3$  and more temporally extensive measurements of leaf  $\text{NH}_3$  emission potentials are particularly needed. For forest ecosystems, a physically representative parameterization for resistance to  $\text{NH}_3$  diffusion through the leaf litter layer and more temporally extensive measurements of the litter  $\text{NH}_3$  emission potential are also needed. Such long-term datasets are also required to assess the interactive effects of changing air quality and climate on both atmosphere-biosphere exchange and ecosystem response to deposition (e.g., Van Houtven et al., 2019). For sensitive ecosystems located in mountainous and other topographically complex landscapes, which includes much of the Class I wilderness area in the U.S., identification of locations suitable for micrometeorological flux measurements will be challenging. Novel flux measurement methods and application of in-situ models, including translation of measurements from more ideal to complex locations, will likely be needed.



### Author Contributions

- 765 1. John T. Walker: Conceptualization, formal analysis, methodology, funding acquisition, project administration, validation, visualization, writing  
2. Xi Chen: Formal analysis, investigation, methodology, validation, writing  
3. Zhiyong Wu: Formal analysis, investigation, methodology, software validation, writing  
4. Donna Schwede: Investigation, formal analysis  
770 5. Ryan Daly: Investigation, formal analysis, validation  
6. Aleksandra Djurkovic: Data curation, investigation, methodology, resources  
7. A. Christopher Oishi: Conceptualization, formal analysis, methodology, validation  
8. Eric Edgerton: Data curation, funding acquisition, formal analysis, methodology, validation, resources  
9. Jesse Bash: Formal analysis, methodology, software  
775 10. Jennifer Knoepp: Data curation, investigation  
11. Melissa Puchalski: Conceptualization, funding acquisition, resources  
12. John Iames: Formal analysis, investigation, writing  
13. Chelcy F. Miniati: Conceptualization, funding acquisition, resources, writing

### Disclaimer

780 The views expressed in this article are those of the authors and do not necessarily represent the views or policies of the U.S. EPA. This study was funded in part by the USDA Forest Service, Southern Research Station, Coweeta Hydrologic Lab. The findings and conclusions in this publication are those of the authors and should not be construed to represent any official USDA or U.S. Government determination or policy.

The authors declare they have no conflict of interest.

### Acknowledgements

785 We gratefully acknowledge field and laboratory support from USDA Forest Service staff at the Coweeta Hydrologic Laboratory, including Christine Sobek, Patsy Clinton, Chuck Marshall, and Cindi Brown. David Kirchgessner (retired, U.S. EPA) tirelessly supported field and laboratory activities during SANDS intensives. Lee Nanny (former U.S. EPA) and Mark Barnes (U.S. EPA) supported field intensives and logistics. We also appreciate the support of Kevin Mishoe (Wood, Inc.) and Christopher Rogers (Wood, Inc.) for support of CASTNET field activities and data management,  
790 respectively.

795



## References

- Altieri, K.E., Turpin, B.J., and Seitzinger S.P., 2009. Composition of dissolved organic nitrogen in continental precipitation investigated by Ultra-High Resolution FT-ICR Mass Spectrometry. *Environmental Science and Technology* 43, 6950-6955.
- 800 Altieri, K.E., Hastings, M.G., Peters, A.J., Sigman, D.M., 2012. Molecular characterization of water soluble organic nitrogen in marine rainwater by ultra-high resolution electrospray ionization mass spectrometry. *Atmospheric Chemistry and Physics* 12, 3557-3571.
- Appel, K.W., Bash, J.O., Fahey, K.M., Foley, K.M., Gilliam, R.C., Hogrefe, C., Hutzell, W.T., Kang, D., Mathur, R., Murphy, B.N., Napelenok, S.L., Nolte, C.G., Pleim, J.E., Pouliot, G.A., Pye, H.O.T., Ran, L., Roselle, S.J., Sarwar, G., Schwede, D. B., Sidi, F.I., Spero, T.L., Wong, D.C., 2021. The Community Multiscale Air Quality (CMAQ) model versions 5.3 and 5.3.1: system updates and evaluation. *Geoscientific Model Development*, 14, 2867–2897.
- 805 Asman, W.A.H., 1995. Parameterization of below-cloud scavenging of highly soluble gases under convective conditions. *Atmospheric Environment*, 29, 1359-1368.
- 810 Bash, J.O., Walker, J.T., Katul, G.G., Jones, M.R., Nemitz, E., Robarge, W.P., 2010. Estimating in-canopy ammonia sources and sinks in a fertilized *Zea mays* field. *Environmental Science and Technology*, 44, 1683-1689.
- Beem, K.B., Raja, S., Schwandner, F.M., Taylor, C., Lee, T., Sullivan, A.P., Carrico, C.M., McMeeking, G.R., Day, D., Levin, E., Hand, J., Kreidenweis, S.M., Malm, W.C., Collett Jr., J.L., 2010. Deposition of reactive nitrogen during the Rocky Mountain Airborne Nitrogen and Sulfur (RoMANS) Study. *Environmental Pollution*, 158, 862-872.
- 815 Benedict, K.B., 2012. Observations of atmospheric reactive nitrogen species and nitrogen deposition in the Rocky Mountains (Thesis). Colorado State University. Libraries.
- Benedict, K.B., Day, D., Schwandner, F.M., Kreidenweis, S.M., Schichtel, B., Malm, W.C., Collett, J.L., 2013. Observations of atmospheric reactive nitrogen species in Rocky Mountain National Park and across northern Colorado. *Atmospheric Environment*, 64, 66-76.
- 820 Blanchard, C.L., Hidy, G.M., 2005. Effects of SO<sub>2</sub> and NO<sub>x</sub> emission reductions on PM<sub>2.5</sub> mass concentrations in the Southeastern United States. *Journal of Air and Waste Management Association*, 55, 265-272.
- Bobbink, R., Hornung M., and Roelofs, J.M., 1998. The effects of air-borne nitrogen pollutants on species diversity in natural and semi-natural European vegetation. *Journal of Ecology*, 86, 717-738.
- 825 Boonstra, R., Krebs, C.J., Cowcill, K., 2017. Responses of key understory plants in the boreal forests of western North America to natural versus anthropogenic nitrogen levels. *Forest Ecology and Management*, 401, 45-54.
- Bragazza, L., Freeman, C., Jones, T., Rydin, H., Limpens, J., Fenner, N., Ellis, T., Gerdol, R., Hajek, M., Iacumin, P., Kutnar, L., Tahvanainen, T., and Toberman, H., 2006. Atmospheric nitrogen deposition promotes carbon loss from peat bogs. *Proceedings of the National Academy of Sciences*, 103, 19386-19389.
- 830 Browne, E.C., Cohen, R.C. 2012 Effects of biogenic nitrate chemistry on the NO<sub>x</sub> lifetime in remote continental regions. *Atmospheric Chemistry and Physics*, 12, 11917–11932, doi:10.5194/acp-12-11917-2012.





- Browne, E.C., Min, K.-E., Wooldridge, P.J., Apel, E., Blake, D.R., Brune, W.H., Cantrell, C.A., Cubison, M.J., Diskin, G.S., Jimenez, J.L., Weinheimer, A.J., Wennberg, P.O., Wisthaler, A., Cohen, R. C., 2013. Observations of total RONO<sub>2</sub> over the boreal forest: NO<sub>x</sub> sinks and HNO<sub>3</sub> sources. *Atmospheric Chemistry and Physics*, 13, 4543–4562.
- 835
- Butler, T., Vermeylen, F., Lehmann, C.M., Likens, G.E., Puchalski, M. 2016. Increasing ammonia concentration trends in large regions of the USA derived from the NADP/AMoN network. *Atmospheric Environment*, 146, 132–140.
- Bytnerowicz, A., Sanz, M.J., Arbaugh, M. J., Padgett, P.E., Jones, D.P., Davila, A., 2005. Passive sampler for monitoring ambient nitric acid (HNO<sub>3</sub>) and nitrous acid (HNO<sub>2</sub>) concentrations. *Atmospheric Environment* 39, 2655–2660.
- 840
- Caldwell, P., Muldoon, C., Ford Miniati, C., et al., 2014. Quantifying the role of National Forest System lands in providing surface drinking water supply for the Southern United States. Gen. Tech. Rep. SRS-197. Asheville, NC: U.S. Department of Agriculture Forest Service, Southern Research Station. 135 p.
- 845
- Cape, J.N., Cornell, S.E., Jickells, T.D., Nemitz, E., 2011. Organic nitrogen in the atmosphere-Where does it come from? A review of sources and methods. *Atmospheric Research* 102, 30–48.
- Chen, F., Dudhia, J., 2001. Coupling an advanced land surface-hydrology model with the Penn State-NCAR MM5 modeling system. Part I: Model implementation and sensitivity. *Monthly Weather Review*, 129, 569–585.
- Chen, X., Walker, J.T., Geron, C., 2017. Chromatography related performance of the Monitor for AeRosols and Gases in ambient air (MARGA): laboratory and field-based evaluation. *Atmospheric Measurement Techniques*, 10, 3893–3908.
- 850
- Chen, X., Xie, M., Hays, M.D., Edgerton, E., Schwede, D., Walker, J.T., 2018. Characterization of organic nitrogen in aerosols at a forest site in the southern Appalachian Mountains. *Atmospheric Chemistry and Physics*, 18, 6829–6846.
- 855
- Clark, C.M., Phelan, J., Doraiswamy, P., Buckley, J., Cajka, J.C., Dennis, R.L., Lynch, J., Nolte, C.G., Spero, T.L., 2018. Atmospheric deposition and exceedances of critical loads from 1800–2025 for the conterminous United States. *Ecological Applications*, 28, 978–1002.
- Coweeta Hydrologic Laboratory 2016. Procedures for chemical analysis. [https://www.srs.fs.usda.gov/coweeta/tools-and-data/wetlab-cookbook\\_revised-2016-01-08.pdf](https://www.srs.fs.usda.gov/coweeta/tools-and-data/wetlab-cookbook_revised-2016-01-08.pdf)
- 860
- David, M., Loubet, B., Cellier, P., Mattsson, M., Schjoerring, J.K., Nemitz, E., Roche, R., Riedo, M., Sutton, M.A., 2009. Ammonia sources and sinks in an intensively managed grassland canopy. *Biogeosciences* 6, 1903–1915.
- Day, D.A., Wooldridge, P.J., Dillon, M. B., Thornton, J.D., and Cohen, R.C., 2002. A thermal dissociation laser-induced fluorescence instrument for in situ detection of NO<sub>2</sub>, peroxy nitrates, alkyl nitrates, and HNO<sub>3</sub>. *Journal of Geophysical Research - Atmospheres*, 107, 4046–4059.
- 865
- Day, D.A., Dillon, M.B., Wooldridge, P.J., Thornton, J.A., Rosen, R.S., Wood, E.C., Cohen, R.C., 2003. On alkyl nitrates, O<sub>3</sub>, and the “missing NO<sub>y</sub>”, *Journal of Geophysical Research - Atmospheres*, 108, 4501.



- Doney, S.C., Mahowald, N., Lima, I., Feely, R.A., Mackenzie, F.T., Lamarque, J-F., Rasch, P.J., 2007. Impact of anthropogenic atmospheric nitrogen and sulfur deposition on ocean acidification and the inorganic carbon system. *Proceedings of the National Academy of Sciences* 104, 14580-14585.
- 870 Ellis, R.A., Jacob, D.J., Sulprizio, M.P., Zhang, L., Holmes, C.D., Schichtel, B.A., Blett, Porter, E., Pardo, L.H., Lynch, J.A., 2013. Present and future nitrogen deposition to national parks in the United States: critical load exceedances. *Atmospheric Chemistry and Physics*, 13, 9083-9095.
- Fahey, K.M. et al., 2017. A framework for expanding aqueous chemistry in the Community Multiscale Air Quality (CMAQ) model version 5.1. *Geoscientific Model Development*, 10, 1587.
- 875 Farmer, D.K., Cohen, R.C., 2008. Observations of HNO<sub>3</sub>, ΣAN, ΣPN and NO<sub>2</sub> fluxes: evidence for rapid HOx chemistry within a pine forest canopy. *Atmospheric Chemistry and Physics*, 8, 3899–3917.
- Flechard, C., Nemitz, E., Smith, R., Fowler, D., Vermeulen, A., Bleeker, A., et al. 2011. Dry deposition of reactive nitrogen to European ecosystems: A comparison of inferential models across the NitroEurope network. *Atmospheric Chemistry and Physics*, 11, 2703–2728.
- 880 Galloway, J.N., Townsend, A.R., Erisman, J.W., Bekunda, M., Cai, Z., Freney, J.R., Martinelli, L.A., Seitzinger, S.P., Sutton, M.A., 2008. Transformation of the nitrogen cycle: recent trends, questions and potential solutions. *Science*, 320, 889-892.
- Giorgi, F., 1986. A particle dry deposition parameterization scheme for use in tracer transport models. *Journal of Geophysical Research - Atmospheres*, 91, 9794-9806.
- 885 Hansen, K., Sørensen, L.L., Hertel, O., Geels, C., Skjøth, C.A., Jensen, B., Boegh, E., 2013. Ammonia emissions from deciduous forest after leaf fall. *Biogeosciences*, 10, 4577–4589.
- Hansen, K., Personne, E., Skjøth, C.A., Loubet, B., Ibrom, A., Jensen, R., Sorenson, L.L., Beogh, E., 2017. Investigation sources of measured forest-atmospheric ammonia fluxes using tow-layer bi-directional modelling. *Agricultural and Forest Meteorology*, 237-238, 80-94.
- 890 Harman, I.N., Finnigan, J.J., 2007. A simple unified theory for flow in the canopy and roughness sublayer. *Boundary Layer Meteorology*, 123, 339-363.
- Hicks, B.B., 2008. On estimating dry deposition rates in complex terrain. *Journal of Applied Meteorology and Climatology*, 47, 1651 – 1658.
- Holland, E.A., Dentener, F.J., Braswell, B.H., Sulzman, J.M. 1999. Contemporary and pre-industrial global reactive nitrogen budgets. *Biogeochemistry*, 46, 7-43.
- 895 Husted, S., Schjoerring, J.K., 1995. Apoplastic pH and ammonium concentration in leaves of *Brassica napus* L. *Plant Physiology*, 1453-1460.
- Jickells, T., Baker, A.R., Cape, J.N., Cornell, S.E., Nemitz, E., 2013. The cycling of organic nitrogen through the atmosphere. *Philosophical Transactions of the Royal Society B* 368, 20130115.
- 900 Keene, W.C., Montag, J.A., Maben, J.R., Southwell, M., Leonard, J., Church, T.M., Moody, J.L., Galloway, J.N., 2002. Organic nitrogen in precipitation over Eastern North America. *Atmospheric Environment*, 36, 4529–4540.
- Kim, P.S., Jacob, D.J., Fisher, J.A., Travis, K., Yu, K., Zhu, L., Yantosca, R.M., Sulprizio, M.P., Jimenez, J.L., Campuzano-Jost, P., Froyd, K.D., Liao, J., Hair, J.W., Fenn, M.A., Butler, C.F., Wagner, N.L., Gordon, T.D.,



- 905 Welti, A., Wennberg, P.O., Crouse, J.D., St. Clair, J.M., Teng, A.P., Millet, D.B., Schwarz, J.P., Markovic, M.Z., and Perring, A.E., 2015 Sources, seasonality, and trends of southeast US aerosol: an integrated analysis of surface, aircraft, and satellite observations with the GEOS-Chem chemical transport model, *Atmospheric Chemistry and Physics*, 15, 10411–10433.
- Knoepp, J.D., Vose, J.M., Swank, W.T., 2008. Nitrogen deposition and cycling across an elevation and vegetation gradient in southern Appalachian forests. *International Journal of Environmental Studies*, 65, 389–408.
- 910 Knoepp, J.D., See, C.R., Vose, J.M., Miniati, C.F., Clark, J.S., 2018. Total C and N pools and fluxes vary with time, soil temperature, and moisture along an elevation, precipitation, and vegetation gradient in southern Appalachian forests. *Ecosystems*, 21, 1623–1638.
- LaCount, M.D., Haeuber, R.A., Macy, T.R., Murray, B.A., 2021. Reducing power sector emissions under the 1990 Clean Air Act Amendments: A retrospective on 30 years of program development and implementation. *Atmospheric Environment*, 245, 118012.
- 915 Laseter, S.H., Ford, C.R., Vose, J.M., Swift, L.W. Jr., 2012. Long-term temperature and precipitation trends at the Coweeta Hydrologic Laboratory, Otto, North Carolina, USA. *Hydrology Research*, 43, 890-901.
- Lavery, T.F., Rogers, C.M., Baumgardner, R., Mishoe, K.P., 2009. Intercomparison of Clean Air Status and Trends Network nitrate and nitric acid measurements with data from other monitoring programs. *Journal of the Air & Waste Management Association*, 59, 214-226.
- 920 Lee, H.-M., Paulot, F., Henze, D. K., Travis, K., Jacob, D. J., Pardo, L. H., Schichtel, B. A. 2016 Sources of nitrogen deposition in Federal Class I areas in the US, *Atmospheric Chemistry and Physics*, 16, 525-540.
- Lehner, M., Rotach, M.W., 2018. Current challenges in understanding and predicting transport and exchange in the atmosphere over mountainous terrain. *Atmosphere*, 9, 276.
- 925 Li, Y., Schichtel, B.A., Walker, J.T., Schwede, D.B., Chen, X., Lehmann, C.M.B., Puchalski, M.A., Gay, D.A., Collett, J.L., 2016. Increasing importance of deposition of reduced nitrogen in the United States. *Proceedings of the National Academy of Sciences*, 113, 5874-5879.
- Lin, M., Walker, J., Geron, C., Khlystov, A., 2010. Organic nitrogen in PM<sub>2.5</sub> aerosol at a forest site in the Southeast US. *Atmospheric Chemistry and Physics*, 10, 2145–2157.
- 930 Lohse, K.A., Hope, D., Sponseller, R., Allen, J.O., Grimm, N.B., 2008. Atmospheric deposition of carbon and nutrients across an arid metropolitan area. *Science of the Total Environment*, 402, 95-105.
- Lynch, J.A., Phelan, J., Pardo L.H., McDonnell, T.C., Clark, C.M., 2017. Detailed Documentation of the National Critical Load Database (NCLD) for U.S. Critical Loads of Sulfur and Nitrogen, version 3.0. National Atmospheric Deposition Program, Illinois State Water Survey, Champaign, IL.
- 935 Makar, P.A., Akingunola, A., Aherne, J., Cole, A.S., Aklilu, Y.-A., Zhang, J., Wong, I., Hayden, K., Li, S.-M., Kirk, J., Scott, K., Moran, M.D., Robichaud, A., Cathcart, H., Baratzedah, P., Pabla, B., Cheung, P., Zheng, Q., Jeffries, D.S., 2018. Estimates of exceedances of critical loads for acidifying deposition in Alberta and Saskatchewan. *Atmospheric Chemistry and Physics*, 18, 9897-9927.
- Massad, R.-S., Nemitz, E., Sutton, M., 2010. Review and parameterisation of bi-directional ammonia exchange  
940 between vegetation and the atmosphere. *Atmospheric Chemistry and Physics*, 10, 10359-10386.



- McDonnell, T.C., Reinds, G.J., Sullivan, T.J., Clark, C.M., Bonten, L.T.C., Mol-Dijkstra, J.P., Wamelink, G.W.W.,  
Dovciak, M., 2018. Feasibility of coupled empirical and dynamic modeling to assess climate change and air  
pollution impacts on temperate forest vegetation of the eastern United States. *Environmental Pollution*, 234, 902-  
914.
- 945 McNulty, S.G., Cohen, E.C., Myers, J.A.M., Sullivan, T.J., Li, H., 2007. Estimates of critical acid loads and  
exceedances for forest soils across the conterminous United States. *Environmental Pollution* 149, 281–292.
- NPS, 2020. National Park Service. Clean Air Status and Trends Network, hourly trace gas data, available at  
[www.epa.gov/castnet](http://www.epa.gov/castnet). Accessed 06/11/2020.
- Meyers, T.P., Hall, M.E., Lindberg, S.E., Kim, K., 1996. Use of the modified Bowen-ratio technique to measure fluxes  
950 of trace gases. *Atmospheric Environment*, 30, 3321 – 3329.
- Neff, J.C., Holland, E.A., Dentener, F.J., McDowell, W.H., Russell, K.M., 2002a. The origin, composition and rates  
of organic nitrogen deposition: A missing piece of the nitrogen cycle? *Biogeochemistry*, 57/58, 99-136.
- Neff, J.C., Townsend, A.R., Gleixner, G., Lehman, S.J., Turnbull, J., Bowman, W., 2002b. Variable effects of nitrogen  
additions on the stability and turnover of soil carbon. *Nature* 419, 915-917.
- 955 Nemitz, E., Sutton, M., Gut, A., San Jose, R., Husted, S., Schjoerring, J., 2000a. Sources and sinks of ammonia within  
an oilseed rape canopy. *Agricultural and Forest Meteorology*, 105, 385–404.
- Nemitz, E., Sutton, M.A., Schjoerring, J.K., Husted, S., Wyers, G.P., 2000b. Resistance modelling of ammonia  
exchange over oilseed rape. *Agricultural and Forest Meteorology*, 10, 405-425.
- Nemitz, E., Milford, C., Sutton, M.A., 2001. A two-layer canopy compensation point model for describing bi-  
960 directional biosphere-atmosphere exchange of ammonia. *Quarterly Journal of the Royal Meteorological Society*,  
127, 815-833.
- Nemitz, E., Sutton, M.A., Wyers, G.P., Jongejan, P.A.C., 2004a. Gas-particle interactions above a Dutch heathland:  
I. Surface exchange fluxes of NH<sub>3</sub>, SO<sub>2</sub>, HNO<sub>3</sub> and HCl. *Atmospheric Chemistry and Physics*, 4, 989-1005.
- Nemitz, E., Sutton, M.A., Wyers, G.P., Otjes, R.P., Mennen, M.G., van Putten, E.M., Gallagher, M.W., 2004b. Gas-  
965 particle interactions above a Dutch heathland: II. Concentrations and surface exchange fluxes of atmospheric  
particles. *Atmospheric Chemistry and Physics*, 4, 1007 – 1024.
- Nilsson, J., Greenfelt, P., 1988. Critical levels for sulphur and nitrogen, 418 pp., Nordic Council of Ministers,  
Copenhagen, Denmark.
- Nouaime, G., Bertman, S.B., Seaver, C., Elyea, D., Huang, H., Shepson, P. B., Starn, T. K., Riemer, D. D., Zika, R.  
970 G., Olszyna, K., 2012. Sequential oxidation products from tropospheric isoprene chemistry: MACR and MPAN  
at a NO<sub>x</sub> -rich forest environment in the southeastern United States. *Journal of Geophysical Research -  
Atmospheres*, 103, 22463–22471.
- Novick, K.A., Walker, J.T., Chan, W.S., Sobek, C., Vose, J., 2013. Eddy covariance measurements with a new fast-  
response, closed-path analyzer: spectral characteristics and cross-system comparisons. *Agricultural and Forest*  
975 *Meteorology*, 181, 17-32.
- Novick, K., Brantley, S., Ford Miniati, C., Walker, J.T., Vose, J., 2014. Inferring the contribution of advection to total  
ecosystem scalar fluxes over a tall forest in complex terrain. *Agricultural and Forest Meteorology*, 185, 1-13.



- Novick, K.A., Oishi, A.C., Miniati, C.F., 2016. Cold air drainage flows subsidize montane valley ecosystem productivity. *Global Change Biology*, 22, 4041-4027.
- 980 Oishi, A.C., Miniati, C.F., Novick, K.A., Brantley, S.T., Vose, J.M., Walker, J.T., 2018. Warmer temperatures reduce net carbon uptake, but not water use in a mature southern Appalachian forest. *Agricultural and Forest Meteorology*, 252, 269-282.
- Ollinger, S.V., Aber, J.D., Reich, P.B., Freuder, R.J., 2002. Interactive effects of nitrogen deposition, tropospheric ozone, elevated CO<sub>2</sub> and land use history on the carbon dynamics of northern hardwood forests. *Global Change*  
985 *Biology*, 8, 545-562.
- Pardo, L.H., Fenn, M.E., Goodale, C.L., Geiser, L.H., Driscoll, C.T., Allen, E.B., Baron, J.S., Bobbink, R., Bowman, W.D., Clark, C.M., Emmett, B., Gilliam, F.S., Greaver, T.L., Hall, S.J., Lilleskov, E.A., Liu, L., Lynch, J.A., Nadelhoffer, K.J., Perakis, S.S., Robin-Abbott, M.J., Stoddard, J.L., Weathers, K.C., Dennis, R.L., 2011. Effects of nitrogen deposition and empirical nitrogen critical loads for ecoregions of the United States. *Ecological*  
990 *Applications* 21, 3049-3082.
- Pardo, L.H., Duarte, N., Van Miegroet, H., Fisher, L.S., Robin-Abbott, M.J., 2018. Critical loads of sulfur and nitrogen and modeled effects of deposition reduction for forested ecosystems of Great Smoky Mountains National Park. Gen. Tech. Rep. NRS-180. Newtown Square, PA: U.S. Department of Agriculture, Forest Service, Northern Research Station. 26 p. <https://doi.org/10.2737/NRS-GTR-180>.
- 995 Paulot, F., Henze, D.K., Wennberg, P.O., 2012. Impact of the isoprene photochemical cascade on tropical ozone, *Atmospheric Chemistry and Physics*, 12, 1307-1325.
- Paulot, F., Jacob, D.J., 2014. Hidden cost of U.S. agricultural exports: particulate matter from ammonia emissions. *Environmental Science and Technology*, 48, 903-908.
- Pearson J., Woodall J., Clough E.C.M., Nielsen K.H., Schjoerring, J.K., 2002. Production and consumption of NH<sub>3</sub> in  
1000 trees. In: Gasche R, Papen H, Rennenberg H (eds) Trace gas exchange in forest ecosystems. Kluwer Academic, The Netherlands, pp 53-77.
- Pleim, J., Ran, L., 2011. Surface flux modeling for air quality applications. *Atmosphere*, 2, 271-302.
- Pleim, J.E., Xiu, A., 1995. Development and testing of a surface flux and planetary boundary layer model for application in mesoscale models. *Journal of Applied Meteorology*, 34, 16-32.
- 1005 Poorter, H., Niinemets, Ü., Poorter, L., Wright, I.J., Villar, R., 2009. Causes and consequences of variation in leaf mass per area (LMA): a meta-analysis. *New Phytologist*, 182, 565-588.
- Nanus, L., McMurray, J.A., Clow, D.W., Saros, J.E., Blett, T., Gurdak, J.J., 2017 Spatial variation of atmospheric nitrogen deposition and critical loads for aquatic ecosystems in the Greater Yellowstone Area. *Environmental Pollution*, 223, 644-656.
- 1010 Root, H.T., Geiser, L.H., Jovan, S., Neitlich, P., 2015. Epiphytic macrolichen indication of air quality and climate in interior forested mountains of the Pacific Northwest, USA. *Ecological Indicators*, 53, 95-105.
- Rumsey, I., Cowen, K., Walker, J.T., Kelley, T.J., Hanft, E.A., Mishoe, K., Rogers, C., Proost, R., Beachley, G.M., Lear, G., Frelink, T., Otjes, R.P., 2014. An assessment of the performance of the Monitor for Aerosols and Gases



- in ambient air (MARGA): a semi-continuous method for soluble compounds. *Atmospheric Chemistry and Physics*, 14, 5639–5658.
- 1015
- Samy, S., Robinson, J., Rumsey, I.C., Walker, J.T., Hays, M.D., 2013. Speciation and trends of organic nitrogen in southeastern U.S. fine particulate matter (PM<sub>2.5</sub>). *Journal of Geophysical Research*, 118, 1996–2006.
- Schneider S., Geßler A., Weber P., von Sengbusch D., Hanemann U., Rennenberg H., 1996. Soluble N compounds in trees exposed high loads of N: a comparison of spruce (*Picea abis*) and beech (*Fagus sylvatica*) grown under field conditions. *New Phytologist*, 134, 103–114.
- 1020
- Schwede, D.B., Lear, G.G., 2014. A novel hybrid approach for estimating total deposition in the United States. *Atmospheric Environment*, 92, 207–220.
- Scudlark, J.R., Russell, K.M., Galloway, J.N., Church, T.M., Keene, W.C., 1998. Organic nitrogen in precipitation at the mid-Atlantic US coast - Methods evaluation and preliminary measurements. *Atmospheric Environment*, 32, 1719–1728.
- 1025
- Shuttleworth, W.J., Wallace, J.S., 1985. Evaporation from sparse crops – an energy combination theory. *Quarterly Journal of the Royal Meteorological Society*, 11, 839–855.
- Sickles II, J.E., Shadwick, D.S., 2015. Air quality and atmospheric deposition in the eastern US: 20 years of change, *Atmospheric Chemistry and Physics*, 15, 173–197.
- 1030
- Slinn, W.G.N., 1982. Predictions for particle deposition to vegetative surfaces. *Atmospheric Environment*, 16, 1785–1794.
- Simkin, S.M., Allen, E.B., Bowman, W.D., Clark, C.M., Belnap, J., Brooks, M.L., Cade, B.S., Collins, S.L., Geiser, L.H., Gilliam, F.S., Jovan, S.E., Pardo, L.H., Schulz, B.K., Stevens, C.J., Suding, K.N., Throop, H.L., and Waller, D.M., 2016. Conditional vulnerability of plant diversity to atmospheric nitrogen deposition across the United States. *Proceedings of the National Academy of Sciences*, 113, 4086–4091.
- 1035
- Sutton, M.A., Asman, W.A.H., Ellermann, T., Van Jaarsveld, J.A., Acker, K., Aneja, V., Duyzer, J., Horvath, L., Paramonov, S., Mitosinkova, M., Tang, Y.S., Achermann, B., Gauger, T., Bartniki, J., Neftel, A., Erisman, J.W., 2003. Establishing the link between ammonia emission control and measurements of reduced nitrogen concentrations and deposition. *Environmental Monitoring and Assessment*, 82, 149–185.
- 1040
- Tang, Y.S., Cape, J.N., Sutton, M.A., 2001. Development and types of passive samplers for monitoring atmospheric NO<sub>2</sub> and NH<sub>3</sub> concentrations. *The Scientific World*, 1, 513–529.
- Toma, S., Bertman, S., Groff, C., Xiong, F., Shepson, P.B., Romer, P., Duffey, K., Wooldridge, P., Cohen, R., Baumann, K., Edgerton, E., Koss, A. R., de Gouw, J., Goldstein, A., Hu, W., Jimenez, J.L., 2019. Importance of biogenic volatile organic compounds to acyl peroxy nitrates (APN) production in the southeastern US during SOAS 2013, *Atmospheric Chemistry and Physics*, 19, 1867–1880.
- 1045
- Trainer, M., Parrish, D.D., Buhr, M.P., Norton, R.B., Fehsenfeld, F.C., Anlauf, K.G., Bottenheim, J.W., Tang, Y.Z., Wiebe, H.A., Roberts, J.M., Tanner, R.L., Newman, L., Bowersox, V.C., Meagher, J.F., Olszyna, K.J., Rodgers, M.O., Wang, T., Berresheim, H., Demerjian, K.L., Roychowdhury, U.K., 1993. Correlation of ozone with NO<sub>y</sub> in photochemically aged air. *Journal of Geophysical Research - Atmospheres*, 98, 2917–2925.



- 1050 U.S. EPA, 2014. U.S. Environmental Protection Agency, 2014. Data from the 2014 National Emissions Inventory, Version 2. Retrieved 2018 from <https://www.epa.gov/air-emissions-inventories/2014-national-emissions-inventory-nei-data>
- U.S. EPA, 2019a. U.S. Environmental Protection Agency Critical Loads Mapper Tool <https://www.epa.gov/air-research/critical-loads-mapper-tool>.
- 1055 U.S. EPA. 2019b. Integrated Science Assessment (ISA) for Oxides of Nitrogen, Oxides of Sulfur and Particulate Matter Ecological Criteria (Final Report). U.S. Environmental Protection Agency, Washington, DC, EPA/600/R-20/278.
- van Houtven, G., Phelan, J., Clark, C., Sabo, R.D., Buckley, J., Thomas, R.Q., et al., 2019. Nitrogen deposition and climate change effects on tree species composition and ecosystem services for a forest cohort. Ecological Monographs, 89, e01345.
- 1060 Walker, J.T., Dombek, T.L., Green, L.A., Gartman, N., Lehmann, C.M.B., 2012. Stability of organic nitrogen in NADP wet deposition samples. Atmospheric Environment, 60, 573-582.
- Walker, J.T., Bell, M.D., Schwede, D., Cole, A., Beachley, G., Lear, G., Wu, Z., 2019a. Aspects of uncertainty in total reactive nitrogen deposition estimates for North American critical load applications. Science of the Total Environment, 690, 1005-1018.
- 1065 Walker, J.T., Beachley, G., Amos, H.M., Baron, J.S., Bash, J., et al. 2019b. Toward the improvement of total nitrogen deposition budgets in the United States. Science of the Total Environment, 691, 1328-1352.
- Walker, J.T., Beachley, G., Zhang, L., Benedict, K.B., Sive, B.C., Schwede, D.B., 2020. A review of measurements of air-surface exchange of reactive nitrogen in natural ecosystems across North America, Science of the Total Environment, 698, 133975.
- 1070 Wang, L., Xu, Y., Schjoerring, J.K., 2011. Seasonal variation in ammonia compensation point and nitrogen pools in beech leaves (*Fagus sylvatica*). Plant Soil, 343, 51-66.
- Weathers, K.C., Simkin, S.M., Lovett, G.M., Lindberg, S.E., 2006. Empirical modeling of atmospheric deposition in mountainous landscapes. Ecological Applications, 16, 1590-1607.
- 1075 Wentworth, G.R., Murphy, J.G., Benedict, K.B., Bangs, E.J., Collett Jr., J.L., 2016. The role of dew as a night-time reservoir and morning source for atmospheric ammonia. Atmospheric Chemistry and Physics, 16, 7435-7449.
- Whitall, D.R., Paerl, H.W., 2001. Spatiotemporal variability of wet atmospheric nitrogen deposition to the Neuse River Estuary, North Carolina. Journal of Environmental Quality, 30, 1508-1515.
- Williams, E.J., Baumann, K., Roberts, J.M., Bertman, S.B., Norton, R.B., Fehsenfeld, F.C., Springston, S.R., 1080 Nunnermacker, L.G., Newman, L., Olszyna, K., Meagher, J., Hartsell, B., Edgerton, E., Perason, J.R., Rodgers, M.O., 1998. Intercomparison of ground-based NO<sub>y</sub> measurements techniques. Journal of Geophysical Research - Atmospheres, 103, 22261-22280.
- Wolfe, G.M., Thornton, J.A., Yatawelli, R.L.N., McKay, M., Goldstein, A.H., LaFranchi, B., Min, K.-E., Cohen, R.C., 2009. Eddy covariance fluxes of acyl peroxy nitrates (PAN, PPN and MPAN) above a Ponderosa pine forest. 1085 Atmospheric Chemistry and Physics, 9, 615-634.



- Xing, J., Pleim, J., Mathur, R., Pouliot, G., Hogrefe, C., Gan, C.-M., Wei, C., 2013. Historical gaseous and primary aerosol emissions in the United States from 1990 to 2010. *Atmospheric Chemistry and Physics*, 13, 7531–7549.
- Yao, X., Zhang, L. 2019. Causes of large increases in atmospheric ammonia in the last decade across North America. *ACS Omega*, 4, 22133-22142.
- 1090 Yi, C., 2008. Momentum transfer within canopies. *Journal of Applied Climatology*, 47, 262-275
- Yu, F., Nair, A.A., Luo, G., 2018. Long-term trend of gaseous ammonia over the United States: Modeling and comparison with observations. *Journal of Geophysical Research - Atmospheres*, 123, 8315–8325.
- Zhang, L., Vet, R., Wiebe, A., Mihele, C., Sukloff, B., Chan, E., Moran, M.D., Iqbal, S., 2008. Characterization of the size-segregated water-soluble inorganic ions at eight Canadian rural sites. *Atmospheric Chemistry and Physics*, 8, 7133-7151.
- 1095 Zhang, R., Thompson, T.M., Barna, M.G., Hand, J.L., McMurray, J.A., Bell, M.D., Malm, W.C., Schichtel, B.A. 2018. Source regions contributing to excess reactive nitrogen deposition in the Greater Yellowstone Area (GYA) of the United States. *Atmospheric Chemistry and Physics*, 18, 12991-13011.

1100

1105

1110

1115

1120





## Tables

**Table 1. Sampling locations and type of sampler deployed.**

Site code	Latitude(N)	Longitude(W)	Elevation(m)	Sampler type
NC25/COW137	35.0605	83.4305	686	AMoN (NC25), CASTNET (COW137), Tisch PM <sub>2.5</sub> <sup>*</sup> , DD-CL, TD-PC-CL, NTN (NC25), EPA precipitation
EFT <sup>a</sup>	35.0591	83.4274	690	MARGA <sup>*</sup> , URG <sup>*</sup> , Passive NH <sub>3</sub> and HNO <sub>3</sub> , micrometeorology
WS18	35.0512	83.4337	806	Passive NH <sub>3</sub> and HNO <sub>3</sub>
SK <sup>b</sup>	35.0482	83.4542	986	Passive NH <sub>3</sub> and HNO <sub>3</sub> , CASTNET (COW005)
CS28	35.0466	83.4650	1189	Passive NH <sub>3</sub> and HNO <sub>3</sub>
CS77	35.0303	83.4604	1425	Passive NH <sub>3</sub> and HNO <sub>3</sub>

<sup>a</sup>-Eddy flux tower; <sup>b</sup>-Screwdriver Knob; <sup>\*</sup> Tisch PM<sub>2.5</sub>, MARGA, and URG denuder/filter pack samplers were deployed only during intensive sampling periods.



**Table 2. Details of intensive and long-term atmospheric measurements at Coweeta.**

Sampler name	Operating periods	Measured species	Resolution	Height (m)*
DD-CL, TD-PCCL	August 2015- August 2016	HNO <sub>3</sub> , NO <sub>y</sub> , ΣAN <sup>1</sup> , ΣPN <sup>2</sup>	Hourly	8
MARGA	Spring, summer 2016 intensives	HNO <sub>3</sub> , NH <sub>3</sub> , NO <sub>3</sub> <sup>-</sup> , SO <sub>4</sub> <sup>2-</sup> , NH <sub>4</sub> <sup>+</sup>	Hourly	~40
URG denuder/filter	All 5 intensives 2015-2016	HNO <sub>3</sub> , NH <sub>3</sub> , NO <sub>2</sub> <sup>-</sup> , NO <sub>3</sub> <sup>-</sup> , SO <sub>4</sub> <sup>2-</sup> , NH <sub>4</sub> <sup>+</sup>	3 or 4-hour integrated	~40
Tisch PM <sub>2.5</sub>	All 5 intensives 2015-2016	NO <sub>2</sub> <sup>-</sup> , NO <sub>3</sub> <sup>-</sup> , SO <sub>4</sub> <sup>2-</sup> , NH <sub>4</sub> <sup>+</sup> , WSTN	24hr integrated	~1
CASTNET (COW137)	Long-term	HNO <sub>3</sub> , NO <sub>3</sub> <sup>-</sup> , SO <sub>4</sub> <sup>2-</sup> , NH <sub>4</sub> <sup>+</sup> , Cl <sup>-</sup> , base cations	Weekly integrated	10
AMoN (NC25)	Long-term	NH <sub>3</sub>	Bi-weekly passive	2
Passive HNO <sub>3</sub> , NH <sub>3</sub>	2015	HNO <sub>3</sub> , NH <sub>3</sub>	Bi-weekly	10 (~40 on EFT)
CASTNET (COW005)	2015	HNO <sub>3</sub> , NO <sub>3</sub> <sup>-</sup> , SO <sub>4</sub> <sup>2-</sup> , NH <sub>4</sub> <sup>+</sup> , Cl <sup>-</sup> , base cations	Weekly integrated	10
NADP/NTN	Long-term	NO <sub>3</sub> <sup>-</sup> , NH <sub>4</sub> <sup>+</sup> , SO <sub>4</sub> <sup>2-</sup> , Cl <sup>-</sup> , H <sup>+</sup> , base cations	Weekly accumulated	Ground
EPA precipitation	February 2015- August 2016	NO <sub>2</sub> <sup>-</sup> , NO <sub>3</sub> <sup>-</sup> , SO <sub>4</sub> <sup>2-</sup> , NH <sub>4</sub> <sup>+</sup> , WSTN	Weekly accumulated	Ground

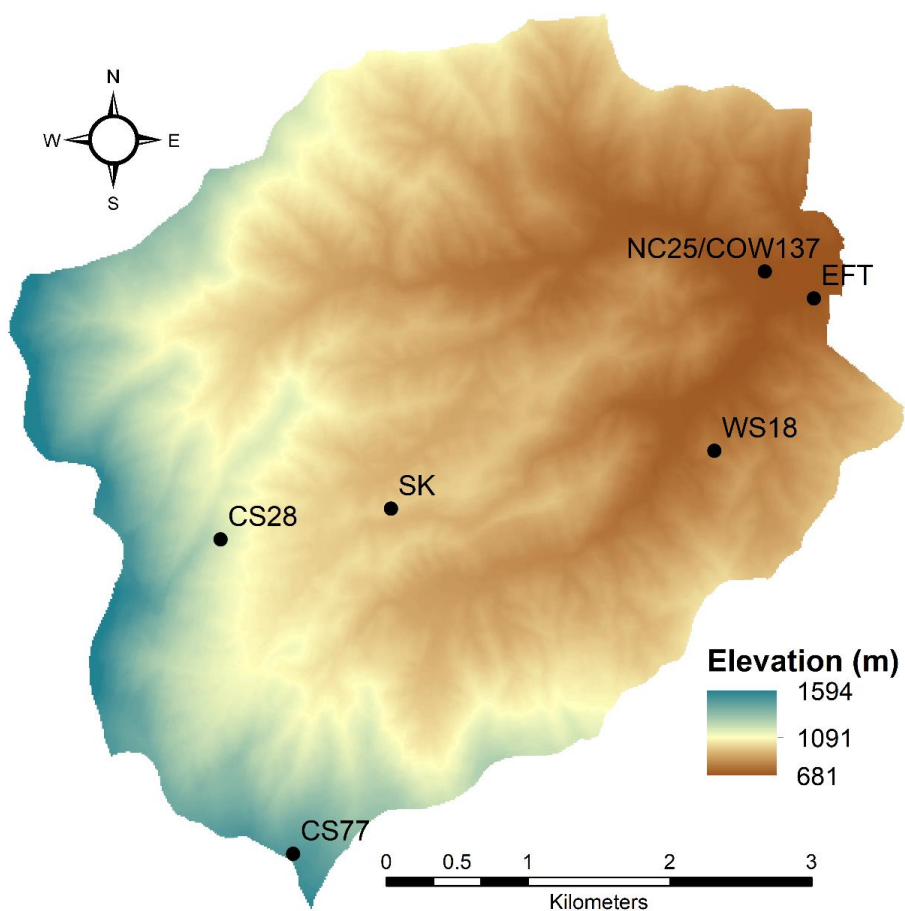
1125 \*Above ground; <sup>1</sup>Total alkylnitrates; <sup>2</sup>Total peroxy-nitrates

**Table 3. Summary of air concentration data sources for STAGE dry deposition modeling.**

Chemical Species	Data Source	Details
NH <sub>3</sub>	Measurement	AMoN measurement with diel profile imposed
HNO <sub>3</sub>	Measurement	Continuous DD-CL
ΣPN	Measurement	Continuous TD-PC-CL. Assume molecular weight (MW = 121.05) of PAN (C <sub>2</sub> H <sub>3</sub> NO <sub>5</sub> )
ΣAN	Measurement	Continuous TD-PC-CL. Assume molecular weight (MW = 136.13) of nitrooxy-butanol (C <sub>4</sub> H <sub>10</sub> NO <sub>4</sub> )
NH <sub>4</sub> <sup>+</sup>	Measurement	CASTNET
NO <sub>3</sub> <sup>-</sup>	Measurement	CASTNET
PON	Estimated based on measured NH <sub>4</sub> <sup>+</sup> + NO <sub>3</sub> <sup>-</sup>	Based on intensive direct measurements, assume PON represents 12% of total PON + NH <sub>4</sub> <sup>+</sup> + NO <sub>3</sub> <sup>-</sup>
NO <sub>2</sub>	Estimated based on measured NO <sub>y</sub>	Based on ratio of NO <sub>2</sub> /NO <sub>y</sub> simulated by CMAQ V5.2.1 at Coweeta



Figures



5

Figure 1. Elevation map of Coweeta Basin with sampling sites in Table 1 indicated.

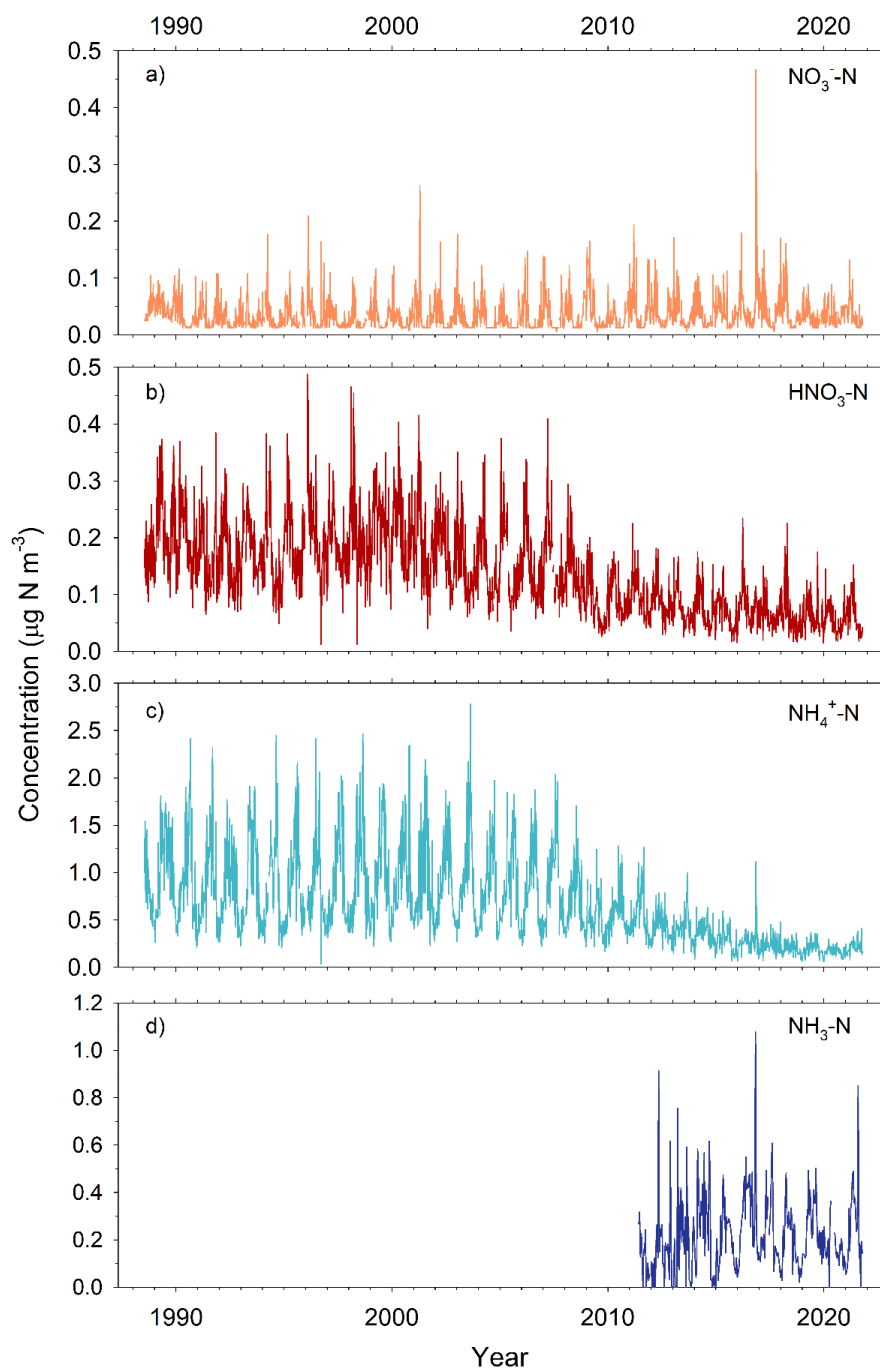


**Figure 2.** Long-term CASTNET (weekly, Site COW137) and AMoN (biweekly, Site NC25) air concentrations (as N) of  $\text{NO}_3^-$  (a),  $\text{HNO}_3$  (b),  $\text{NH}_4^+$  (c) and  $\text{NH}_3$  (d).

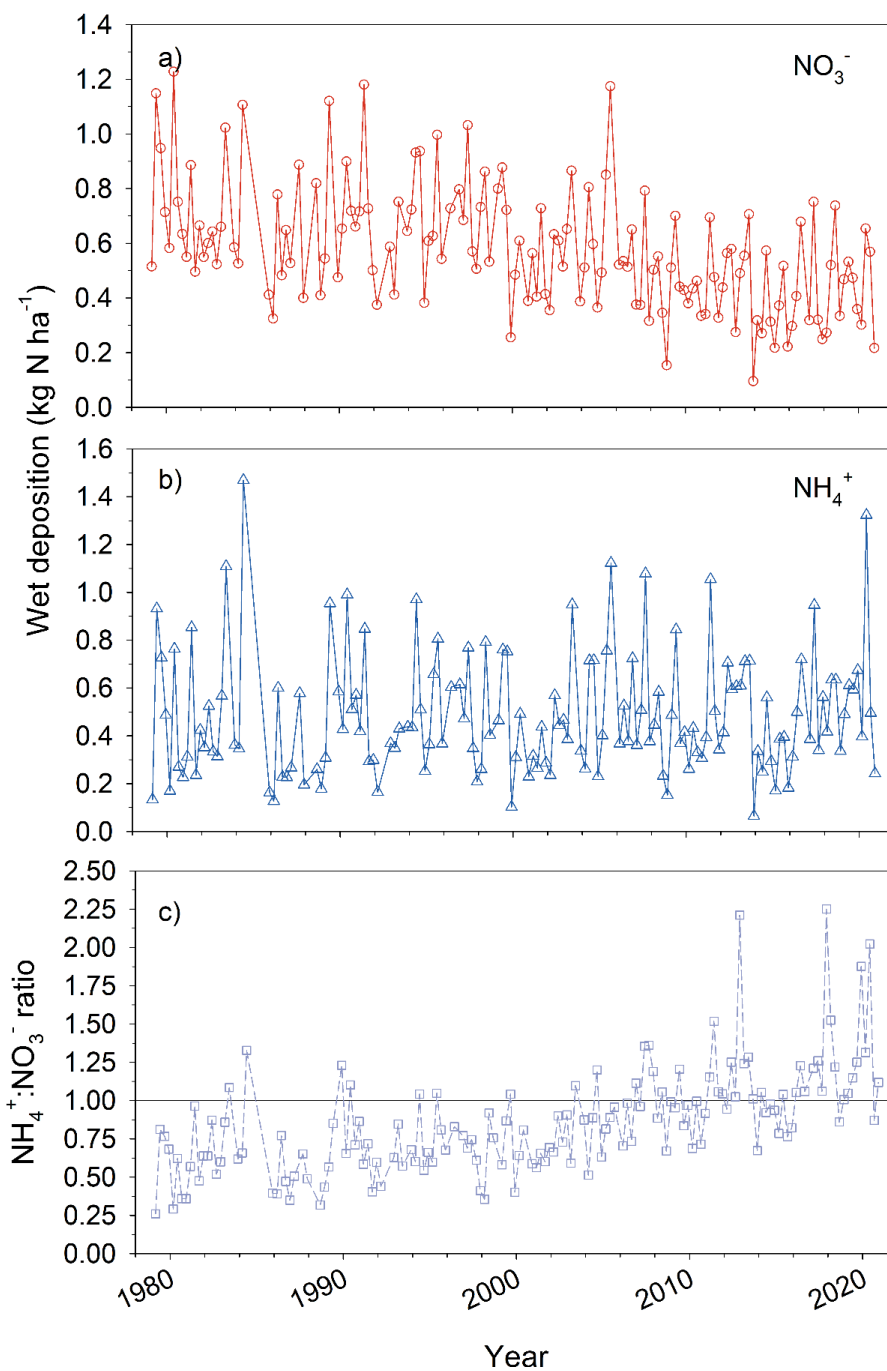


Figure 3. Long-term NTN NC25 measurements of seasonal  $\text{NH}_4^+$  (a) and  $\text{NO}_3^-$  (b) wet deposition along with the ratio of  $\text{NH}_4^+$  to  $\text{NO}_3^-$  as nitrogen and 1:1 reference line (c).

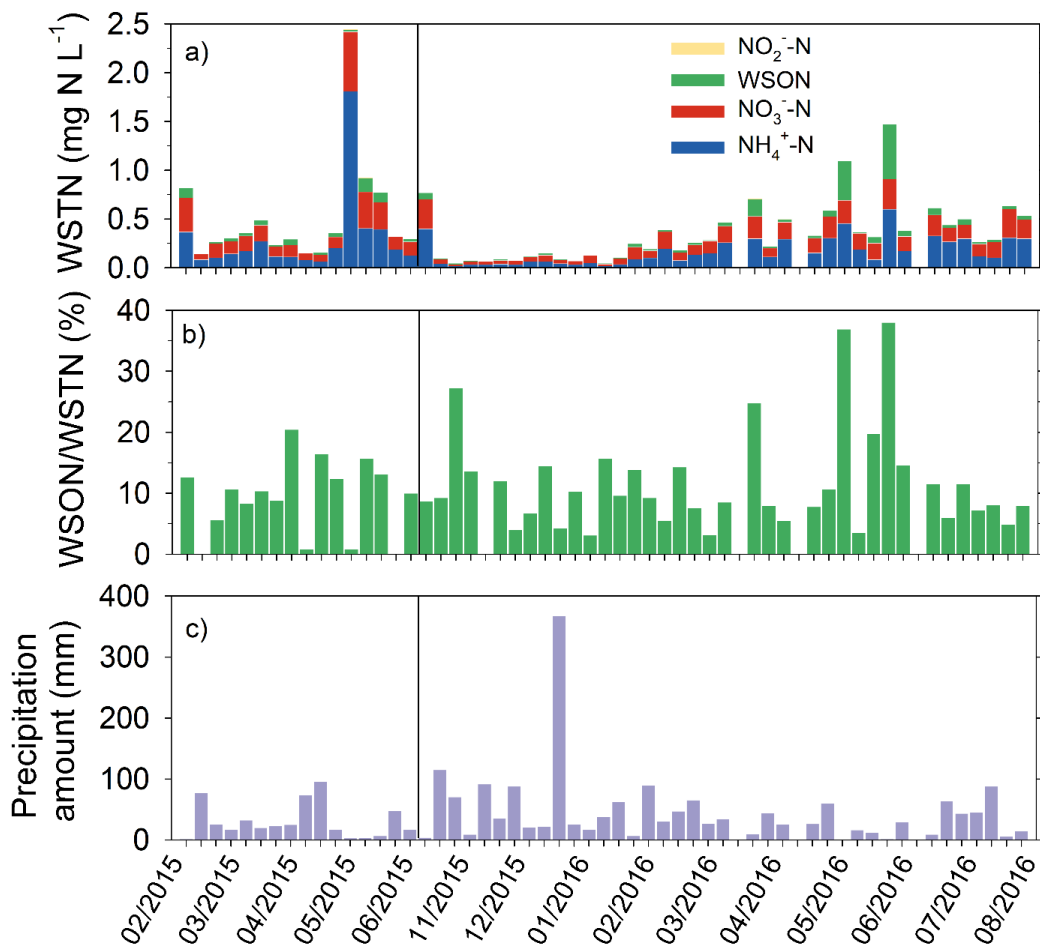


Figure 4. Concentrations of nitrogen species in weekly precipitation samples (a), percentage contribution of WSON to WSTN in precipitation (b), and precipitation amount (c). Vertical line marks discontinuity due to missing data from 06/01/2015 to 10/19/2015.

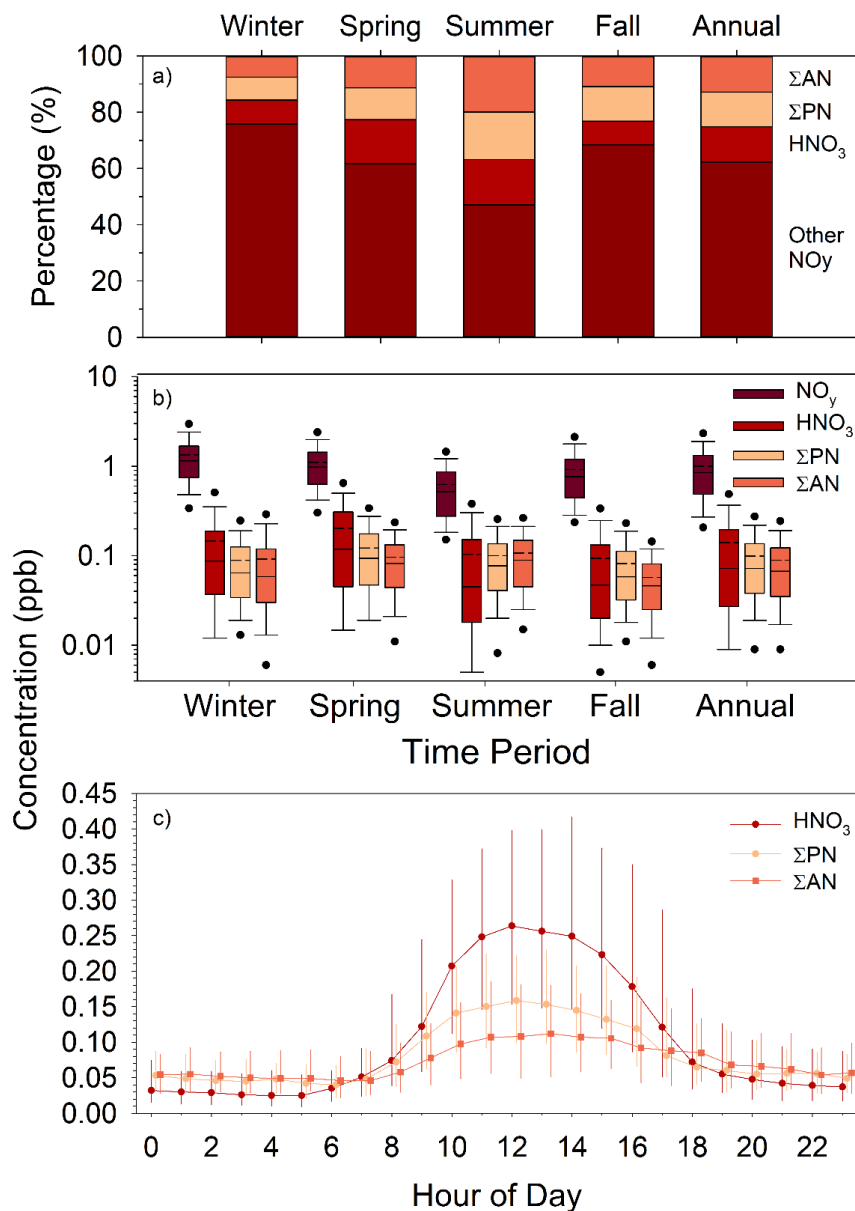


Figure 5. Seasonal and annual % contribution of HNO<sub>3</sub>, ΣPN, ΣAN, and other compounds to total NO<sub>y</sub> (a); seasonal and annual boxplots of NO<sub>y</sub>, HNO<sub>3</sub>, ΣPN and ΣAN where solid and dashed lines inside box represent median and mean, respectively; top and bottom of box represent 75<sup>th</sup> and 25<sup>th</sup> percentiles; whiskers represent 10<sup>th</sup> and 90<sup>th</sup> percentiles, and dots represent 5<sup>th</sup> and 95<sup>th</sup> percentiles (b); and diel profiles of HNO<sub>3</sub>, ΣPN, and ΣAN where observations represent median hourly concentration and bars represent the interquartile range (c). “Other NO<sub>y</sub>” is calculated as NO<sub>y</sub> – HNO<sub>3</sub> – ΣPN – ΣAN which, while primarily comprised of NO<sub>x</sub>, includes N<sub>2</sub>O<sub>5</sub>, HONO, NO<sub>3</sub>, and possibly other organics.

5

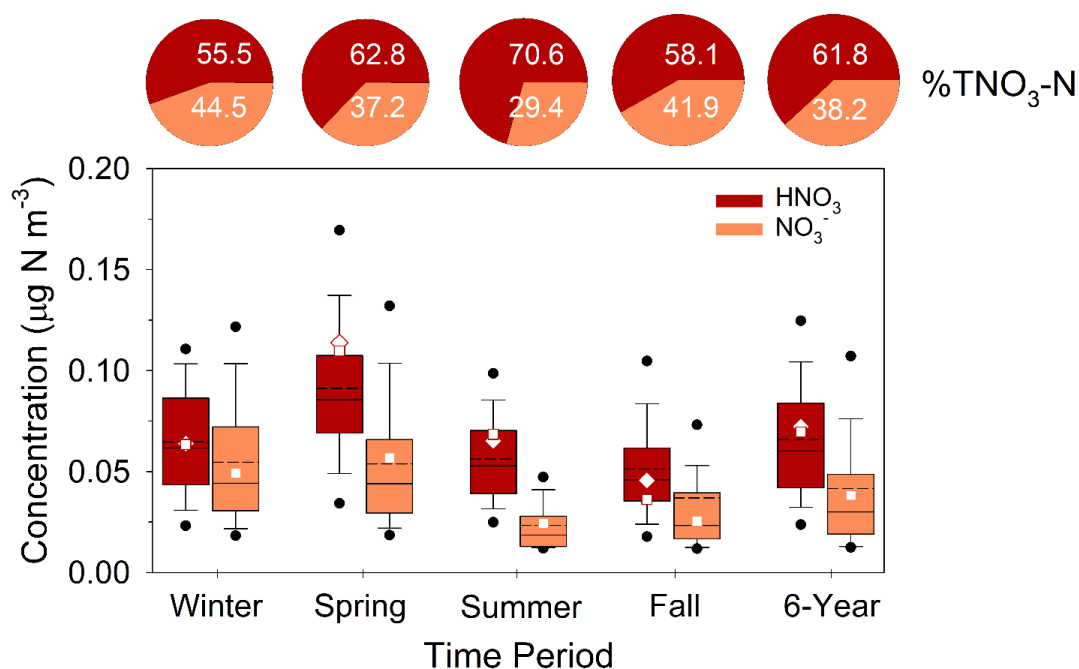


Figure 6. Summary of CASTNET HNO<sub>3</sub> and NO<sub>3</sub><sup>-</sup> concentrations (as N) from 2015-2020 during winter, spring, summer and fall. Solid and dashed lines inside box represent median and mean, respectively. Top and bottom of box represent 75<sup>th</sup> and 25<sup>th</sup> percentiles. Whiskers represent 10<sup>th</sup> and 90<sup>th</sup> percentiles and dots represent 5<sup>th</sup> and 95<sup>th</sup> percentiles. “6-Year” represents the statistics for the entire 6-Year period. Squares and diamonds represent the seasonal and annual mean CASTNET (HNO<sub>3</sub> and NO<sub>3</sub><sup>-</sup>) and continuous DD-CL HNO<sub>3</sub> for the August 2015 – August 2016 modeling period, respectively. Pie charts represent average % contribution of HNO<sub>3</sub> and NO<sub>3</sub><sup>-</sup> to total NO<sub>3</sub><sup>-</sup> (HNO<sub>3</sub> + NO<sub>3</sub><sup>-</sup>) expressed as nitrogen.

5

10



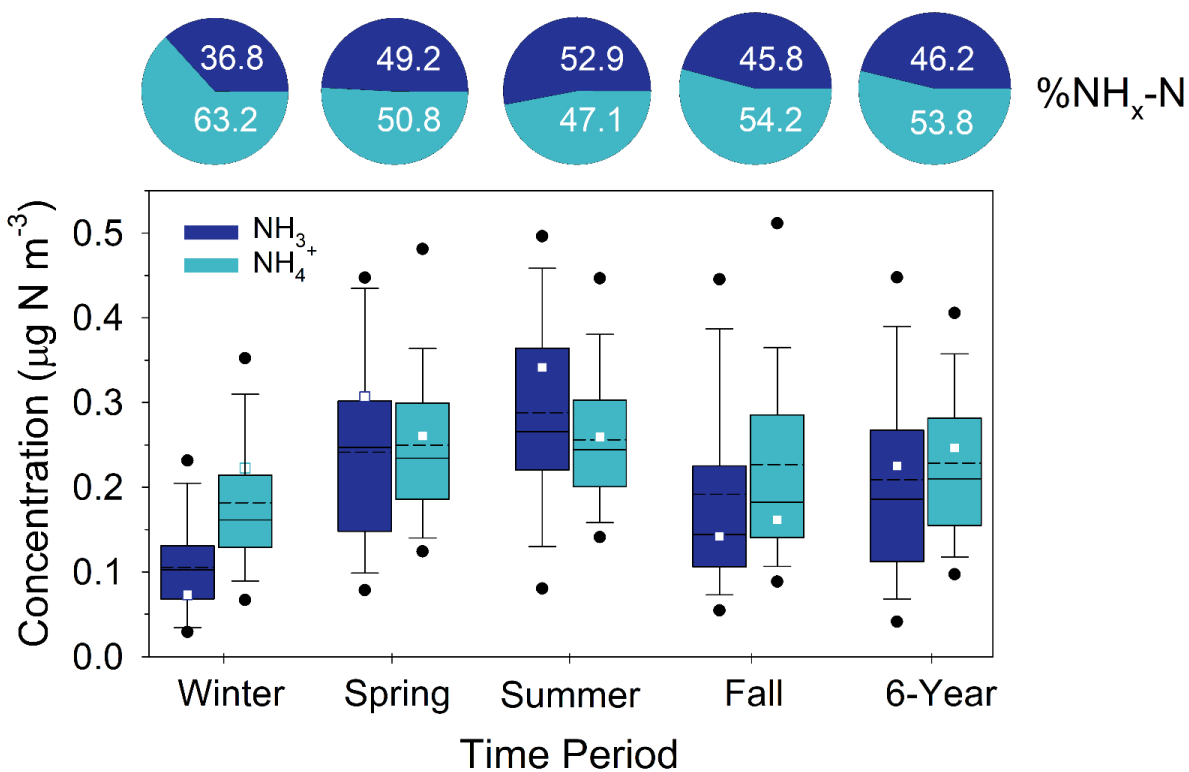


Figure 7. Summary of AMoN NH<sub>3</sub> and CASTNET NH<sub>4</sub><sup>+</sup> concentrations (as N) from 2015-2020 during winter, spring, summer and fall. Solid and dashed lines inside box represent median and mean, respectively. Top and bottom of box represent 75<sup>th</sup> and 25<sup>th</sup> percentiles. Whiskers represent 10<sup>th</sup> and 90<sup>th</sup> percentiles and dots represent 5<sup>th</sup> and 95<sup>th</sup> percentiles. “6-Year” represents the statistics for the entire 6-Year period. Squares represent the seasonal and annual mean concentration for the August 2015 – August 2016 modeling period. Pie charts represent average % contribution of NH<sub>3</sub> and NH<sub>4</sub><sup>+</sup> to total NH<sub>x</sub> (NH<sub>3</sub>+NH<sub>4</sub><sup>+</sup>) expressed as nitrogen. AMoN concentrations were adjusted by subtracting the mean travel blank for the 6-year period, equivalent to 0.09 µg N m<sup>-3</sup>, and applying a factor of 0.92 to account for the effect of higher elevation/lower pressure at Coweeta on the sampler diffusion coefficient.

5

10

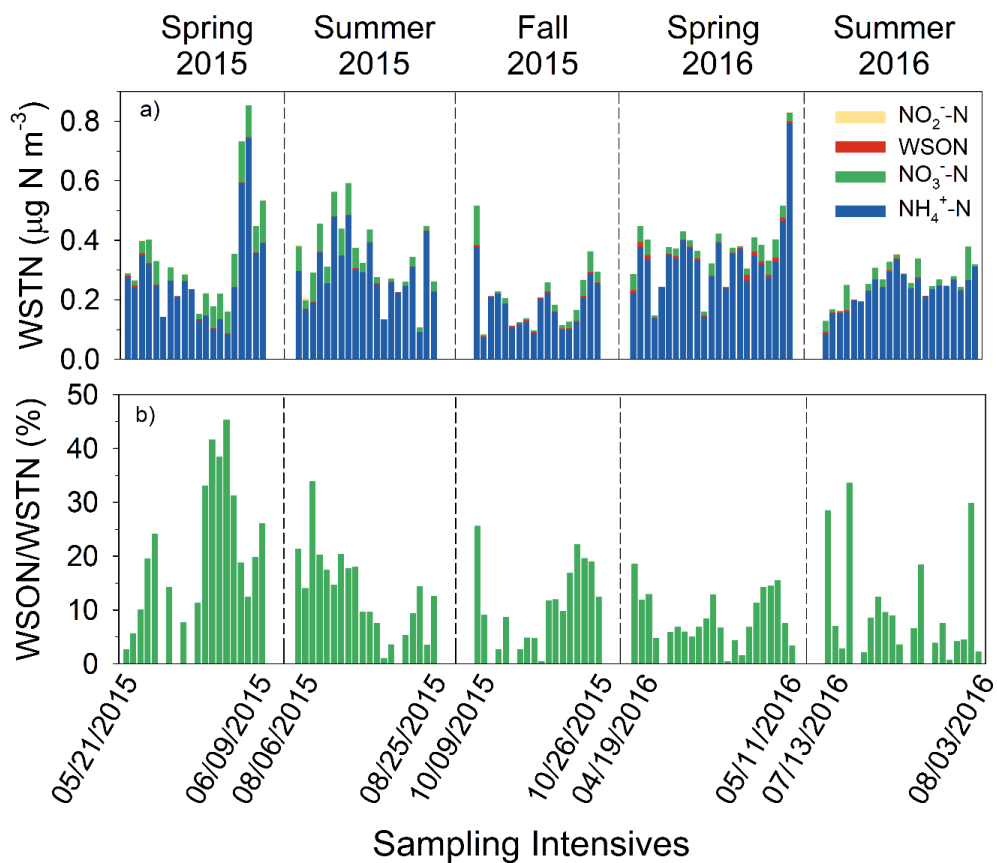
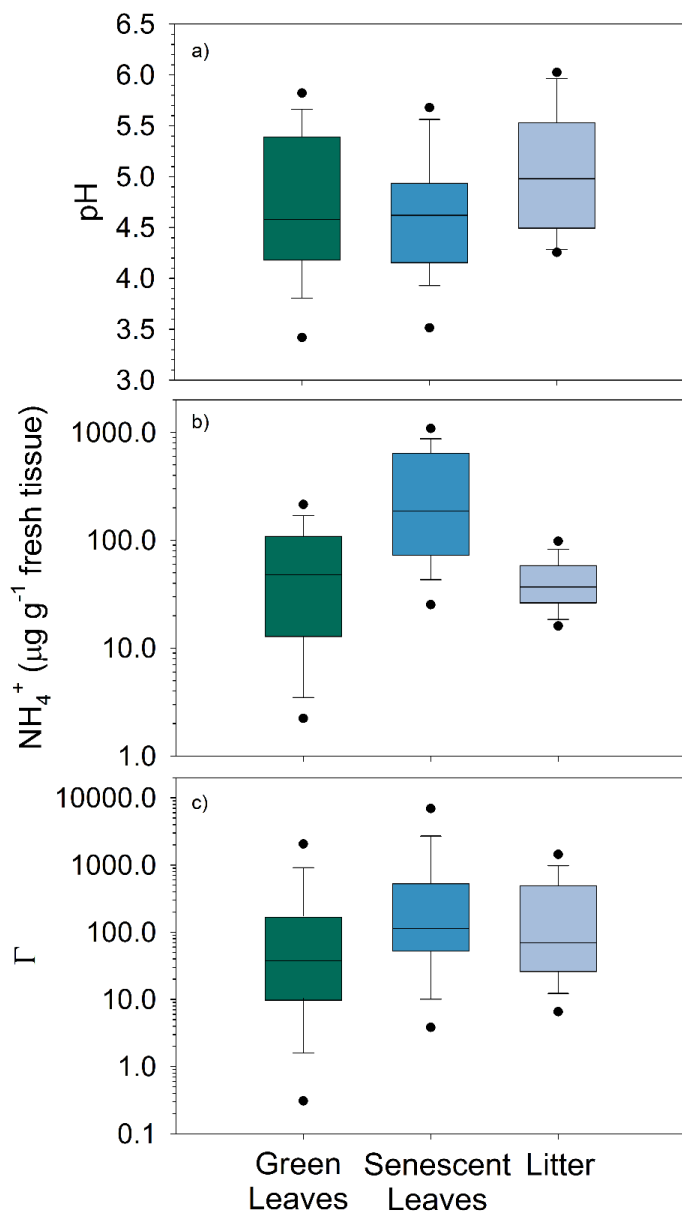


Figure 8. Contributions of N species to WSTN in 24-hour Hi-Vol  $\text{PM}_{2.5}$  samples during seasonal SANDS intensives (a) along with percentage of WSON to WSTN (b).



**Figure 9.** Boxplots of pH (a),  $\text{NH}_4^+$  (b) concentration ( $\mu\text{g g}^{-1}$  fresh tissue), and equivalent emission potential ( $\Gamma$ ) (c) in tissue of green leaves, senescent leaves, and litter on the forest floor. Solid line inside box represents median. Top and bottom of box represent 75<sup>th</sup> and 25<sup>th</sup> percentiles. Whiskers represent 10<sup>th</sup> and 90<sup>th</sup> percentiles and dots represent 5<sup>th</sup> and 95<sup>th</sup> percentiles.

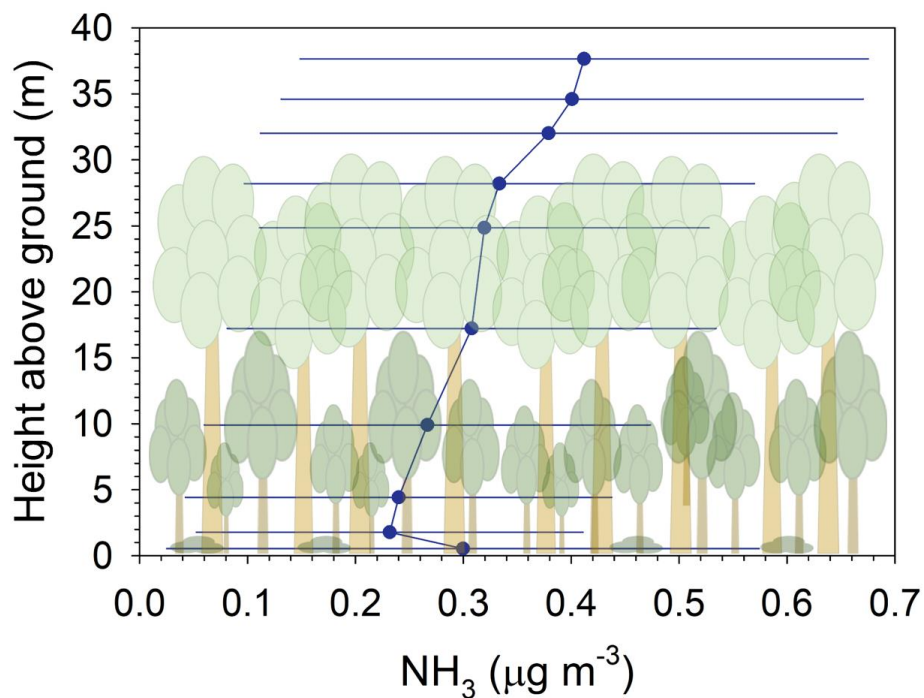


Figure 10. Vertical concentration profiles of NH<sub>3</sub>. Mean (filled circle) and standard deviation (bars) of concentrations are shown for  $N = 76$  daytime profiles.

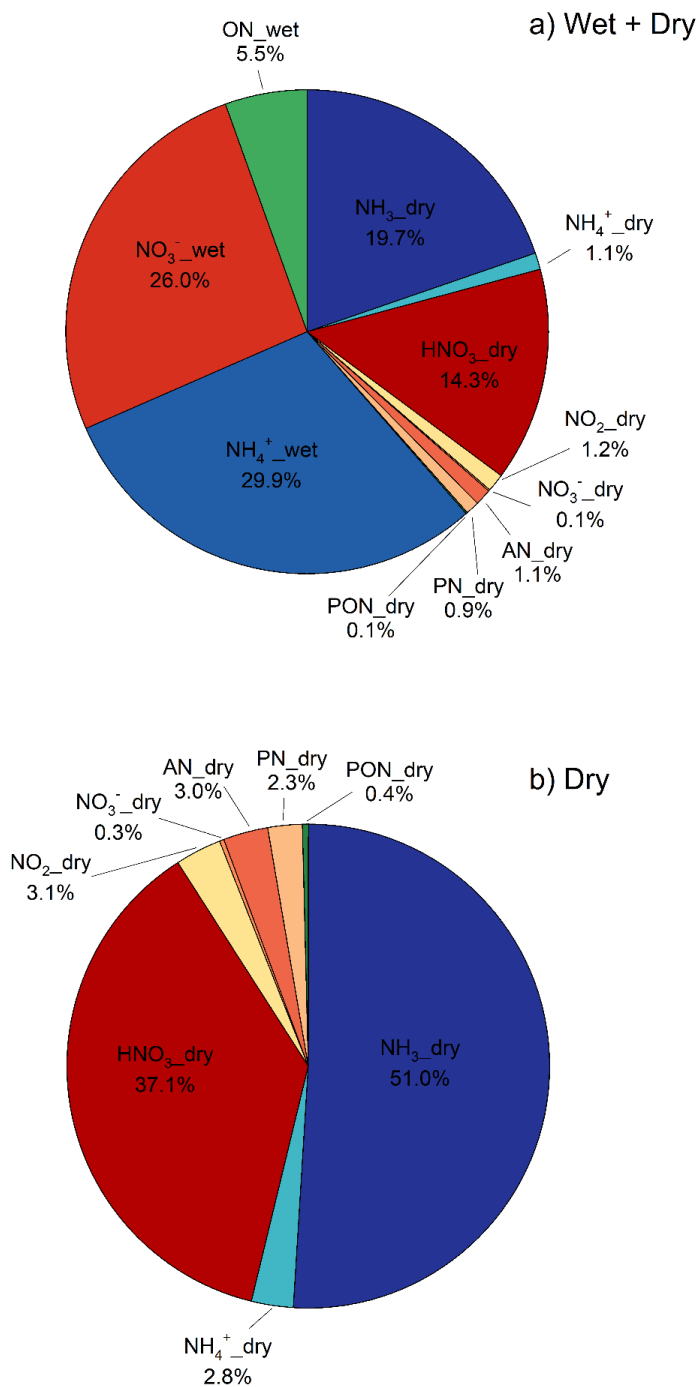


Figure 11. Speciated annual total (wet and dry) (a) and dry (b) deposition showing percent contribution of individual components.

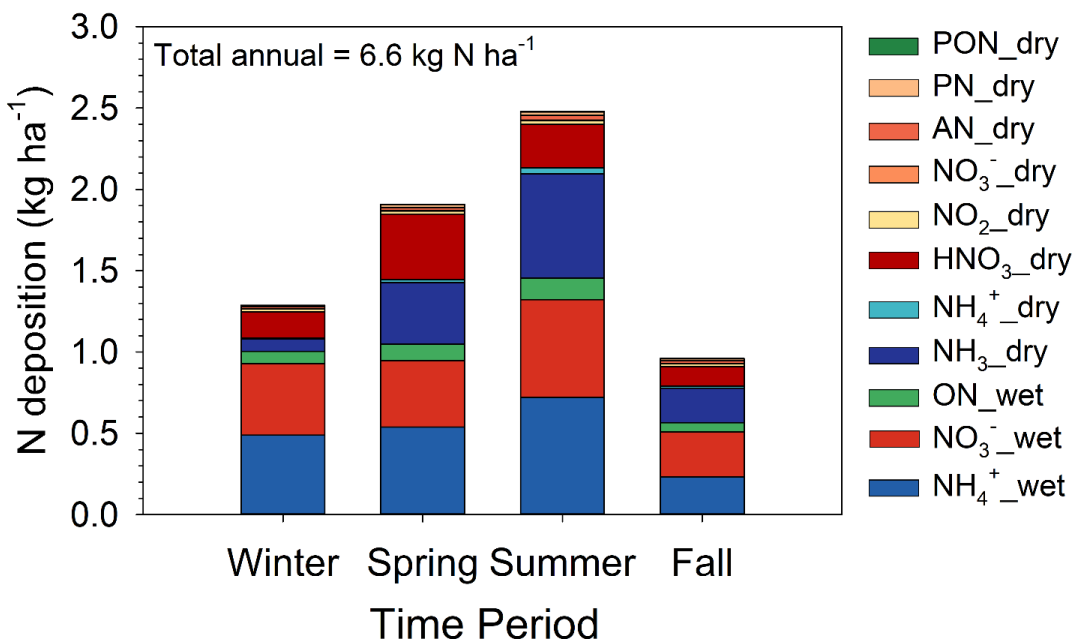
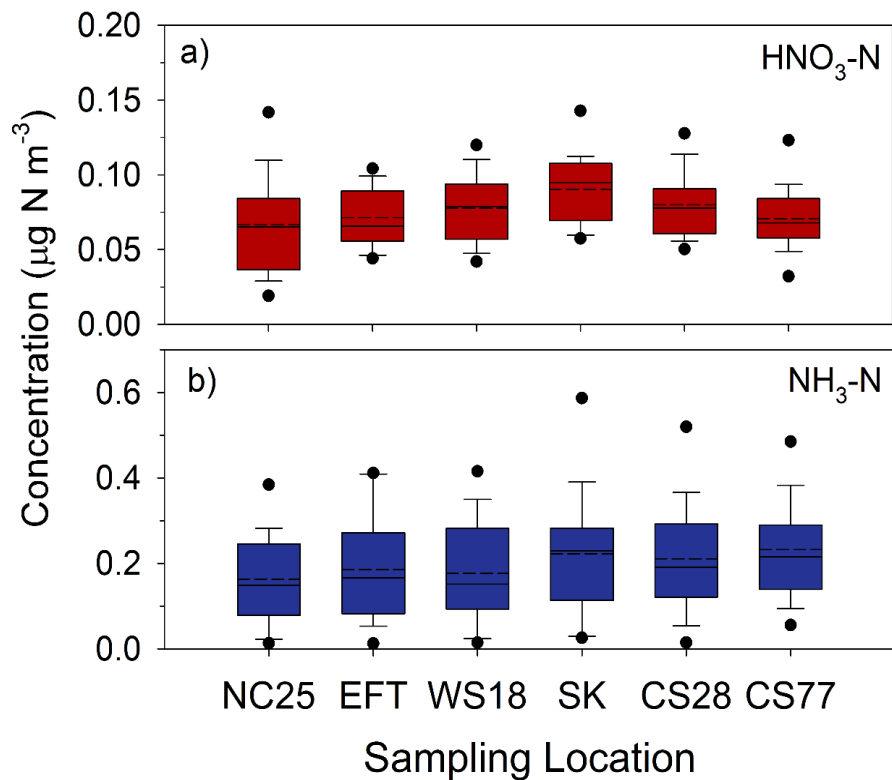


Figure 12. Seasonal speciated deposition budget. Nr species are listed in the legend as defined in the text, along with indication of the deposition pathway (dry or wet).



5 **Figure 13.** Concentrations (as N) of HNO<sub>3</sub> (a) and NH<sub>3</sub> (b) measured at different elevations, increasing from left to right (see Figure 1 and Table 1), across the Coweeta Basin. Solid and dash lines inside box represent median and mean, respectively. Top and bottom of box represent 75<sup>th</sup> and 25<sup>th</sup> percentiles. Whiskers represent 90<sup>th</sup> and 10<sup>th</sup> percentiles and dots represent 95<sup>th</sup> and 5<sup>th</sup> percentiles.